https://doi.org/10.5194/egusphere-2025-5752
Preprint. Discussion started: 4 December 2025

Soil thermal memory regulates event-scale precipitation recycling lag in a dryland environment

Ruolin Li[1,2,3], Yang Cui[4] and Qi Feng[1,2,3]

[1] Key Laboratory of Ecological Safety and Sustainable Development in Arid Lands, Lanzhou 730000, China
[2] Qilian Mountains Eco-Environment Research Center in Gansu Province, Lanzhou 730000, China
[3] Key Laboratory of Ecohydrology of Inland River Basin, Northwest Institute of Eco- Environment and Re-sources, Chinese Academy of Sciences, Lanzhou 730000, China
[4] Ningxia Hui Autonomous Regional Meteorological Observatory. Yinchuan 75002, China

Correspondence to: Yang Cui (cuiyang@cma.gov.cn) & Qi Feng (qifeng@lzb.ac.cn)

https://doi.org/10.5194/egusphere-2025-5752
Preprint. Discussion started: 4 December 2025

Abstract. Precipitation events in dryland environments generate sharp but uneven adjustments in surface and atmospheric conditions. While the atmosphere recovers rapidly from rainfall-induced cooling, the soil retains a substantial portion of the cooling anomaly, creating a land-surface memory. Using multi-year, multi-layer observations from five stations in Ningxia, China, and ERA5 reanalysis, this study investigates how this soil thermal memory timescale (τ_{rec}) modulates the timing of recycled moisture return.

Analysis of 112 events reveals a consistent "cold-humid pulse" with rapid atmospheric recovery but slow soil recovery, whose persistence we quantify as τ_{rec} (20–80 hours) using an exponential-decay framework. ERA5 diagnostics show the recycled moisture signal peaks 20–40 hours after rainfall, defining a recycling lag (τ_{RR}). Event-wise analysis of ten long-duration events reveals a systematic positive correlation ($R \approx 0.57$) between τ_{rec} and τ_{RR}.

Longer soil memory consistently predicts a more delayed recycling peak. We show this relationship is mediated by enhanced moisture-heat feedback (H), where persistent cold soils slow boundary-layer recovery and postpone the reactivation of evaporation. These results identify soil thermal memory as an active regulator; the timing of recycled moisture is not solely an atmospheric process but is partially land-controlled. This work establishes a novel "coupling-memory-recycling" pathway, providing a new mechanism for understanding and modeling dryland precipitation dynamics.

1 Introduction

Drylands and semi-arid regions occupy more than one third of the global land surface and exert strong influence on regional hydrology, ecosystem functioning, and climate variability (D'Odorico and Bhattachan, 2012; Maestre et al., 2016; Palmquist et al., 2016; Schumacher et al., 2022; Wang et al., 2012). These environments are characterised by intense solar radiation, sparse vegetation, low humidity, and large diurnal temperature ranges, all of which contribute to a surface energy regime that is highly sensitive to short-term disturbances (Feldman et al., 2019; Schumacher et al., 2022). As a consequence, land–atmosphere interactions in drylands often display rapid and pronounced responses to precipitation, boundary-layer development, and cloud cover (Catalano et al., 2016; Gu et al., 2025). While much work has examined these interactions at seasonal to interannual timescales, the event-scale processes that govern how the land surface and atmosphere respond to individual rainfall episodes remain less well understood (Abel et al., 2020; Guillod et al., 2015; Moore et al., 2021; Yin and Porporato, 2024).

Substantial research has advanced theories of soil moisture–temperature coupling and its impacts on boundary-layer growth, convective triggering, and precipitation persistence (Hsu et al., 2024; Rahmati et al., 2024; Robinson et al., 2016; Schwingshackl et al., 2018; Yang et al., 2018). Recycling studies have likewise identified local evaporation fractions and large-scale moisture pathways (Adloff et al., 2022; Hauser et al., 2019; Keys et al., 2012; Li et al., 2024; McHugh et al., 2015). However, this research has focused on climatological or synoptic averages, overlooking the hourly to sub-daily evolution of rainfall disturbances (Dunkerley, 2019; Quichimbo et al., 2021; Sippel et al., 2017). In particular, how the land surface mediates the *timing* of recycled moisture return post-event has received limited attention, as most studies implicitly attribute such lags to atmospheric transport rather than land-surface processes (Abel et al., 2020; Gandhi et al., 2025).

This gap is notable because rainfall events induce sharp, spatially coherent perturbations to surface temperature, humidity, and energy partitioning (Guillod et al., 2015; Klein and Taylor, 2020). Rain onto a hot, dry surface creates an abrupt temperature drop and humidity surge—a "cold–humid pulse" (Hu et al., 2021; Zhang et al., 2019). While the atmosphere recovers within hours, the shallow soil retains this cooling anomaly, warming slowly via conduction and radiation (Miralles et al., 2019). This persistence constitutes a 'soil thermal memory', whose influence on post-rain boundary-layer development and evaporation recovery remains underexplored (Rahmati et al., 2024; Stacke and Hagemann, 2016). Such memory could delay surface heating and evaporation (Guillod et al., 2015), thereby modulating the timing of local moisture return and influencing event-scale precipitation recycling.

Investigating this requires a region with strong radiative forcing, low humidity, and sharp pre- versus post-rainfall contrasts. Central Ningxia in Northwest China provides such a setting, defined by intense solar heating, efficient nocturnal cooling, and sparse vegetation that amplify surface–atmosphere thermal gradients (Chen et al., 2021; Li et al., 2023; Moch et al., 2022; Ren et al., 2022; Wu et al., 2024). Intermittent convective precipitation often follows prolonged dry, decoupled periods (Fu et al., 2016; Hou, 2022; Lu et al., 2019; Ma et al., 2021; Zhang et al., 2021). 5 national meteorological stations offer a unique platform with high-frequency, multi-layer soil (down to 320 cm), grass, and air temperature measurements, ideal for resolving the vertical structure and recovery of thermal anomalies. Combining this dense in situ record with ERA5 reanalysis (providing the atmospheric recycling component) enables a detailed examination of event-scale land–atmosphere coupling.

This study establishes how rainfall reorganises near-surface thermodynamic conditions and how soil thermal memory influences recycled moisture timing. We first characterise the cold–humid pulse using ±72 h composites across 112 events, examining its variance with intensity. We then quantify the soil thermal memory timescale (τ_{rec}) using an exponential-decay framework, assessing its seasonal and cross-station persistence. Using ERA5, we compute hourly precipitation recycling rates to define the recycling lag (τ_{RR}). Finally, analysing ten long-duration events, we evaluate the τ_{rec}–τ_{RR} association and its mediation by surface–atmosphere coupling indices.

The remainder of this paper is organised as follows. Section 2 introduces the study region, station measurements, and reanalysis data used in the analysis. Section 3 describes the methodological framework, including the derivation of thermodynamic variables, the detection of precipitation events, the construction of composite anomalies, the estimation of soil thermal memory, and the calculation of recycling metrics. Section 4 presents the results, covering the characteristic rainfall-induced cold–humid pulse, the seasonal behaviour of soil thermal memory, and the event-scale linkage between τ_{rec} and τ_{RR}. Section 5 discusses the physical interpretation of these findings within the broader context of land–atmosphere coupling and moisture recycling. Section 6 summarizes the key conclusions and outlines directions for future work.

2 Study Area and Data

2.1 Study Area

The study region is central Ningxia, Northwest China (37–40°N, 105–107°E; Fig. 1a). This domain, a transition zone between the East Asian monsoon margin and the arid interior, has a semi-arid climate with strong radiative forcing, sparse vegetation, and pronounced thermal amplitudes (Chi et al., 2023; Tan et al., 2011; Zhao et al., 2014). The five national stations (53518, 53603, 53610, 53614, 53618) share uniform topography (1099–1130 m), limiting orographic influence on local energy and moisture exchange.

https://doi.org/10.5194/egusphere-2025-5752
Preprint. Discussion started: 4 December 2025

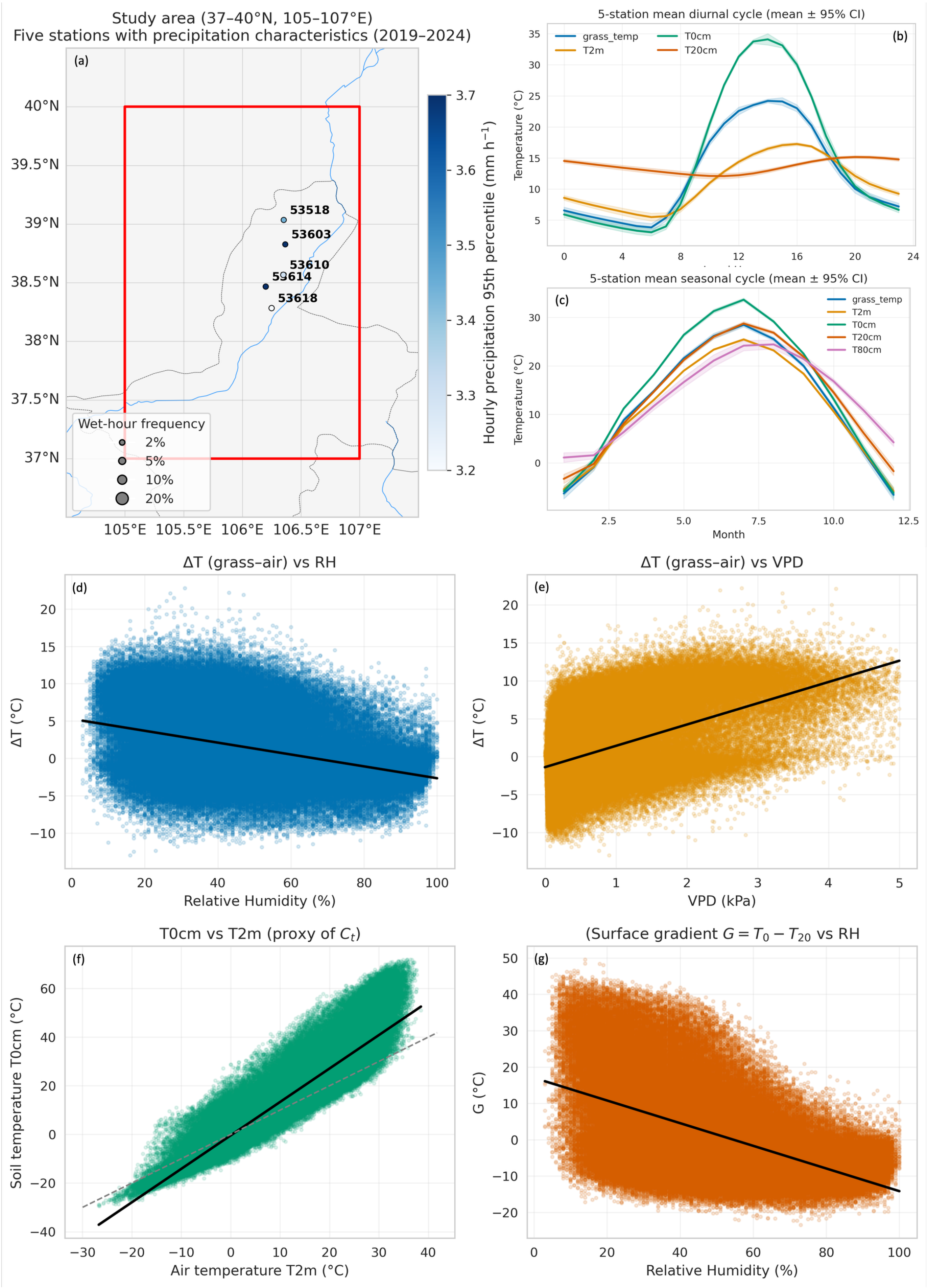

Figure 1. Study area and overall surface–atmosphere thermal–moisture characteristics in the Ningxia region (37–40° N, 105–107° E). (a) Location of the five national meteorological stations with their mean hourly precipitation characteristics during 2019–2024. Circle color indicates the 95th-percentile hourly precipitation intensity (mm h⁻¹), and circle size represents the wet-hour frequency (> 0.1 mm h⁻¹, %). (b) Five-station mean diurnal temperature cycle (2020–2024, mean ± 95 % CI) for grass, air, and soil layers. (c) Five-station mean seasonal temperature cycle (mean ± 95 % CI) from surface to deep soil (0–80 cm). (d–g) Key coupling and constraint relationships derived from hourly observations: (d) Grass–air temperature difference (ΔT) versus relative humidity (RH); (e) ΔT versus vapor-pressure deficit (VPD); (f) Soil-air temperature coupling (T_{0cm} vs T_{2m}, proxy of C_t); (g) Surface thermal gradient G versus RH.

Ningxia's climate is dominated by intense warm-season solar heating and efficient nocturnal radiative cooling, especially under clear, dry conditions (Chi et al., 2023; Qian and Lin, 2004). These factors produce one of northern China's largest diurnal temperature ranges and promote strong near-surface thermal gradients. Limited vegetation and shallow rooting depth further enhance surface sensitivity to radiative forcing, enabling rapid land surface responses to atmospheric moisture and cloudiness (Cao et al., 2023; Gao et al., 2017; Wang et al., 2022).

Precipitation is intermittent, concentrated in short-lived, warm-season convective events. With modest annual totals (200–300 mm yr⁻¹), rain events frequently follow prolonged dry periods when the land surface is overheated and decoupled from the atmosphere(Cao et al., 2023; Chi et al., 2023; Zhao et al., 2014). Consequently, these events impose abrupt thermal and moisture perturbations that penetrate the upper soil and reorganize surface energy partitioning(Li et al., 2022).

These regional characteristics—strong radiative forcing, low humidity, and event-driven precipitation—produce clear expressions of surface cooling, soil thermal memory, and delayed recycling responses, making Ningxia an ideal laboratory to quantify how land-surface thermal anomalies evolve and feed back onto event-scale atmospheric moisture pathways.

2.2 Station Observations

Hourly in situ observations from five national stations (53518, 53603, 53610, 53614, 53618) form the core land-surface dataset. Located within a 60 km north–south corridor in central Ningxia (Fig. 1a), these stations share similar elevation (1099–1130 m), land cover (semi-arid steppe and cropland mosaic), and climate regimes. This homogeneous setting enables multi-station aggregation to identify regional-scale land–atmosphere processes.

2.2.1 Variables and instrumentation

The stations report a comprehensive suite of near-surface hydro-meteorological variables at hourly resolution, including:

Table 1. Overview of near-surface hydro-meteorological variables measured at the five national stations (hourly resolution)

Category	Variable	Description
Air temperature	T_{2m}	Air temperature at 2 m above ground
Surface temperature	T_{grass}	Grass/surface skin temperature from infrared radiometer

Category	Variable	Description
Soil temperature	$T_{0}cm$, $T_{5}cm$, $T_{10}cm$, $T_{15}cm$, $T_{20}cm$, $T_{40}cm$, $T_{80}cm$, $T_{160}cm$, $T_{320}cm$	Soil temperature profile at nine depths
Humidity	*RH*, vapor pressure	Relative humidity and actual vapor pressure
Precipitation	*P*	Tipping-bucket or optical precipitation measurement
Wind	Wind speed, wind direction	Hourly wind measurements
Evaporation	Pan evaporation	Station pan evaporation
Miscellaneous	Visibility, metadata	Visibility and station ancillary parameters

Such vertically resolved temperature measurements are critical for analysing the radiative–conductive structure of the land surface and for quantifying the recovery of rainfall-induced cooling at multiple depths (Table 1), which underpins the soil thermal memory metric (τ_{rec}) used later in the analysis.

2.2.2 Temporal coverage and harmonisation

The observational period spans 2019-12-31 21:00 to 2024-12-31 20:00, yielding a multi-year, continuous record suitable for event-scale and seasonal diagnostics. All timestamps were converted to UTC+8 to ensure alignment with ERA5-derived recycling metrics (which were originally provided in UTC). The five station datasets were merged into a unified, station-labelled hourly archive.

2.2.3 Quality control and preprocessing

A multi-step quality control procedure was applied prior to analysis:

1. **Physical range screening** for temperature, *RH*, and precipitation to remove impossible or instrument-error values.
2. **Temporal consistency checks**, identifying and correcting discontinuities arising from sensor resets or transmission gaps.
3. **Vertical consistency checks** for soil temperature, ensuring realistic monotonicity with depth and removing isolated spikes at individual layers.
4. **Daily completeness filtering**, requiring ≥18 valid hours per day for all composite and correlation calculations.

Derived variables used in subsequent analyses—**vapor pressure deficit (*VPD*)**, **grass–air temperature difference (ΔT)**, and **soil thermal gradient (*G*)**—were computed directly from these quality-controlled hourly measurements.

The final dataset provides a robust, high-frequency, multi-layer description of surface and subsurface thermal–moisture states. This observational foundation enables the event-focused analyses in Sections 4 and 5, including the construction of composite cold–humid pulses, the estimation of soil thermal memory, and the evaluation of land–atmosphere coupling metrics.

2.3 ERA5 Reanalysis

To characterize atmospheric transport and quantify precipitation recycling processes beyond the capability of local station measurements, we complemented the in situ observations with the ERA5 global atmospheric reanalysis (The ERA5 global reanalysis). ERA5 provides physically consistent, hourly, three-dimensional fields of winds, humidity, and surface fluxes, which are essential for deriving the moisture recycling metrics used in this study.

2.3.1 Dataset description

ERA5 data were obtained at 0.25° × 0.25° spatial resolution and hourly temporal resolution for the same period as the station record (2020–2024) (ERA5 hourly data on pressure levels from 1940 to present; ERA5 hourly data on single levels from 1940 to present). The following variables were extracted to support the recycling analysis:

- Total precipitation
- Surface evaporation
- Near-surface specific humidity, relative humidity, and temperature
- u- and v-component winds
- Boundary-layer and column-integrated moisture fields
- Auxiliary pressure and flux variables

These fields provide the necessary inputs for diagnosing local moisture recycling, which requires simultaneous information on evaporation, atmospheric humidity, and horizontal moisture flux divergence—parameters that cannot be obtained from station measurements alone.

2.3.2 Time handling and alignment

ERA5 timestamps are reported in UTC, whereas station observations are recorded in UTC+8. To ensure consistent temporal alignment—crucial for calculating the recycling lag τ_{RR}—ERA5 variables and the derived recycling ratio were shifted by +8 hours to match the station-based event timeline. This alignment ensures that the precipitation peak time ($\tau = 0$ h) is strictly synchronised between ERA5 and the surface observations.

2.3.3 Recycling ratio (ρ)

The precipitation recycling ratio (ρ) was computed from ERA5 using a moisture budget–based formulation that quantifies the fractional contribution of local evaporation to precipitation (the specific calculation process is shown in section 3.5). For each event, ρ was extracted as a continuous time series centred around the station-identified precipitation peak.

2.3.4 Rationale for combining ERA5 with station observations

ERA5 serves as the atmospheric counterpart to the detailed surface record from the five stations. While the stations provide high-quality measurements of energy and moisture exchange at the land surface and within the soil column, **they cannot resolve atmospheric transport**, vertical moisture flux divergence, or the spatial pathway of recycled moisture. ERA5 fills this gap by providing:

- Regionally coherent moisture and wind fields
- Hourly evaporation and precipitation budgets
- Dynamical consistency needed for diagnosing ρ and τ_{RR}

This combined station–reanalysis approach is therefore essential for linking land-surface thermal memory (τ_{rec}) to the timing and magnitude of recycled moisture contributions.

3. Methods

3.1 Derived thermodynamic and coupling variables

From the quality-controlled hourly observations, we derived a set of variables describing near-surface thermodynamic conditions and land–atmosphere coupling.

3.1.1 Vapor pressure deficit (*VPD*)

VPD was calculated as the difference between saturation vapor pressure at T_{2m} and the observed vapor pressure(Chai et al., 2018).

$$e = e_{sat}(T_{2m}) \tag{1}$$

$$VPD = e_{sat}(T_{2m}) - e \tag{2}$$

It characterises atmospheric moisture demand and responds rapidly to rainfall-induced cooling and humidification (Lu et al., 2022).

3.1.2 Grass–air temperature difference (ΔT)

ΔT is defined as:

https://doi.org/10.5194/egusphere-2025-5752
Preprint. Discussion started: 4 December 2025

$$\Delta T = T_{grass} - T_{2m} \tag{3}$$

ΔT measures the surface–air thermal contrast and indicates the degree of radiative heating versus evaporative cooling. Rainfall typically reduces *ΔT* through rapid humidification (Lu et al., 2022).

3.1.3 Soil thermal gradient (*G*)

G is defined as:

$$G = T_{0cm} - T_{20cm} \tag{4}$$

G represents shallow soil stratification and is sensitive to rain-driven surface cooling and its downward propagation (Brunetti et al., 2022).

3.1.4 Soil–air temperature coupling coefficient (C_t)

C_t is defined as:

$$C_t = Corr(T_{0cm}, T_{2m}) \tag{5}$$

C_t quantifies co-variability between soil and air temperature and indicates the strength of land–atmosphere thermal linkage during an event (Hsu et al., 2024).

3.1.5 Moisture–heat feedback index (*H*)

H is defined as:

$$H = Corr(RH, \Delta T) \tag{6}$$

, which *RH* is relative humidity, captures how humidity regulates surface–air temperature contrast. Strong positive values indicate efficient moisture–energy coupling following rainfall (Hsu et al., 2024).

Together these diagnostics characterize the structure and recovery of the surface thermal–moisture state.

3.2 Precipitation event detection

Hourly station precipitation was used to identify rainfall events. An event was defined as a continuous period in which hourly precipitation exceeded 0.1 mm h^{-1}. Events were separated by at least two consecutive dry hours to avoid merging independent episodes. For each event, the hour of maximum precipitation (p_{peak}) was taken as $\tau = 0$.

Events were detected for each of the five stations and then combined into a unified catalogue, preserving local variability in rainfall intensity and soil response. A total of 112 events satisfied detection criteria.

Events were further divided into strong and weak groups based on the median P_{peak} to examine intensity-dependent responses.

For all analyses (composites, τ_{rec}, τ_{RR}, coupling metrics), variables were extracted over a symmetric ±72 h window around $\tau = 0$. This window consistently captures the sharp atmospheric adjustment, subsequent soil recovery, and the delayed recycling response.

A subset of 10 long events (duration ≥ 140 h) was selected to ensure sufficient pre- and post-rainfall coverage for estimating both soil thermal memory and recycling lag. These include five strong and five weak cases spanning different seasons (Table 2).

Table 2. List of the ten long-duration precipitation events selected for analysing the relationship between soil thermal memory (τ_{rec}) and the recycling lag (τ_{RR}). For each event, the table reports the start and end times (in both UTC+8 and UTC), the peak precipitation time, event duration, peak hourly intensity (P_{peak}), and total accumulated rainfall (P_{sum}). Events are grouped into five strong cases and five weak cases based on peak precipitation intensity. These long-duration events provide the necessary temporal extent for jointly evaluating post-rainfall soil-temperature recovery and the delayed response of recycled moisture.

Case	Start (UTC+8)	Start (UTC)	End (UTC+8)	End (UTC)	Peak (UTC+8)	Peak (UTC)	Duration (h)	P_{peak} (mm/h)	P_{sum}
Strong Cases									
1	2024-08-06 01:00	**2024-08-05 17:00**	2024-08-13 01:00	**2024-08-12 17:00**	2024-08-08 17:00	**2024-08-08 09:00**	144	12.88	60
2	2024-08-22 05:00	**2024-08-21 21:00**	2024-08-29 07:00	**2024-08-28 23:00**	2024-08-25 01:00	**2024-08-24 17:00**	150	10.36	204.5
3	2024-08-31 12:00	**2024-08-31 04:00**	2024-09-08 20:00	**2024-09-08 12:00**	2024-09-04 01:00	**2024-09-03 17:00**	204	8.02	170.2
4	2022-07-08 15:00	**2022-07-08 07:00**	2022-07-15 15:00	**2022-07-15 07:00**	2022-07-11 04:00	**2022-07-10 20:00**	180	10.82	151.7
5	2024-04-16 04:00	**2024-04-15 20:00**	2024-04-23 04:00	**2024-04-22 20:00**	2024-04-18 20:00	**2024-04-18 12:00**	168	5.42	139.4
Weak Cases									
6	2021-04-21 20:00	2021-04-21 12:00	2021-04-28 20:00	2021-04-28 12:00	2021-04-24 12:00	2021-04-24 04:00	180	1.56	49.8
7	2023-08-08 19:00	2023-08-08 11:00	2023-08-15 19:00	2023-08-15 11:00	2023-08-11 08:00	2023-08-11 00:00	192	1.72	37.1
8	2021-09-04 11:00	2021-09-04 03:00	2021-09-06 23:00	2021-09-06 15:00	2021-09-05 12:00	2021-09-05 04:00	192	1.40	27.2
9	2020-09-10 21:00	2020-09-10 13:00	2020-09-17 21:00	2020-09-17 13:00	2020-09-13 10:00	2020-09-13 02:00	180	1.82	25.8

Case	Start (UTC+8)	Start (UTC)	End (UTC+8)	End (UTC)	Peak (UTC+8)	Peak (UTC)	Duration (h)	P_{peak} (mm/h)	P_{sum}
10	2023-09-06 02:00	2023-09-05 18:00	2023-09-13 02:00	2023-09-12 18:00	2023-09-08 17:00	2023-09-08 09:00	168	1.24	22.8

3.3 Composite anomaly analysis

Composite analysis was used to characterize the average thermodynamic response to rainfall.

For each event, variables were extracted over ±72 h and converted to anomalies relative to a pre-event baseline defined over −72 to −48 h. The anomaly for variable $x'(\tau)$ is:

$$x'(\tau) = x(\tau) - \bar{x}_{\text{baseline}}. \tag{7}$$

Composites were obtained as the across-event mean of $x'(\tau)$. Strong and weak events were composited separately to examine intensity dependence. Confidence intervals were estimated using the standard error of the mean.

This framework captures both the rapid atmospheric response and the slower soil recovery, and provides the foundation for estimating τ_{rec} and comparing events of different intensities.

3.4 Estimation of soil thermal memory (τ_{rec})

The soil thermal memory timescale τ_{rec} was derived from the recovery of the 0 cm soil temperature anomaly. The surface layer responds most clearly and consistently to rainfall and exhibits a well-defined relaxation curve suitable for timescale estimation.

For each event, the post-peak cooling recovery (τ = 0–72 h) of T_{0cm} anomalies was fitted using a single-exponential function:

$$T' * 0cm(\tau) \approx Aexp\left(-\frac{\tau}{\tau_{rec}}\right) + B, \tag{8}$$

where

- A is the anomaly amplitude at $\tau = 0$,
- B is a small residual offset,
- τ_{rec} is the e-folding recovery time.

Non-linear least squares fitting was applied, and events with well-behaved recovery ($R^2 \geq 0.3$) were retained. The e-folding time τ_{rec} provides a consistent measure of the persistence of rainfall-induced cooling (Brunetti et al., 2022).

Seasonal and station-level statistics of τ_{rec} were obtained by aggregating event-wise timescales with bootstrap confidence intervals.

3.5 Recycling Ratio and Recycling Lag (τ_{RR})

To link land-surface thermal anomalies with subsequent atmospheric moisture return, we quantified the precipitation recycling rate (ρ) using ERA5 reanalysis. The recycling diagnostics follow a physically based two-reservoir moisture-tracking

https://doi.org/10.5194/egusphere-2025-5752
Preprint. Discussion started: 4 December 2025

framework (local vs. advected vapor, Keys et al., 2014; Tuinenburg and Staal, 2020; Van Der Ent et al., 2014), implemented at hourly resolution over the domain 38–39.5°N, 106–107°E for 2020–2024. This approach distinguishes the fraction of precipitation originating from local evaporation versus that transported by large-scale advection, enabling event-scale analysis of moisture recycling dynamics.

3.5.1 Calculation of the recycling ratio (ρ)

ERA5 hourly fields—including evaporation, total precipitation, specific humidity, horizontal winds, and pressure—were processed on all pressure levels. Column water vapor was partitioned into:

- ($W_{\text{loc}}(x, y, p, t)$): vapor mass of local origin
- ($W_{\text{adv}}(x, y, p, t)$): vapor mass of advected origin

At the initial step, all atmospheric moisture was assumed advected (($W_{\text{adv}} = W_{\text{tot}}$), ($W_{\text{loc}} = 0$)), after which the two reservoirs evolve prognostically through:

1. Surface evaporation input to (W_{loc})
2. Precipitation removal, partitioned proportionally to the column fraction of locally sourced vapor
3. Horizontal advection, computed using an upwind finite-difference scheme applied separately to u and v wind components
4. Mass conservation, with negative values clipped to zero and domain-integrated water-mass budgets checked for stability

The local precipitation amount at each hour is the area integral of P_{loc}, and the hourly recycling rate is defined as:

$$\rho(t) = \frac{\sum_{x,y} P_{\text{loc}}(x, y, t)}{\sum_{x,y} P_{\text{tot}}(x, y, t)}. \tag{9}$$

Numerical stability checks (CFL condition) and non-negativity constraints ensured physically consistent evolution. Daily ρ values were obtained by summing hourly (P_{loc}) and (P_{tot}) over valid hours (≥18 h) before taking their ratio.

3.5.2 Temporal alignment with station-based precipitation

ERA5 times are reported in UTC and were converted to UTC+8 to align with the station-defined event timeline. This alignment is essential because the recycling lag (τ_{RR}) depends on the correct timing of both the precipitation peak and the ρ peak.
For each of the ten long-duration precipitation events (Section 3.2.5), the ρ time series was extracted over a ±72 h window around the station-identified precipitation peak.

3.5.3 Definition of the recycling lag (τ_{RR})

The recycling lag quantifies how long after the rainfall peak the recycled moisture signal reaches its maximum. It is defined as:

$$\tau_{RR} = t(\rho_{\max}) - t(P_{\text{peak}}), \tag{10}$$

where

- ($t(P_{\text{peak}})$): station-observed peak precipitation time
- ($t(\rho_{\max})$): time of the maximum recycling rate (ρ)

Because ρ typically rises only after post-rain evaporation and boundary-layer recovery resume, τ_{RR} represents a dynamical response timescale integrating land-surface conditions and atmospheric transport.

3.5.4 Role of τ_{RR} in the coupling–memory–recycling framework

The recycling lag provides the atmospheric complement to the soil-based thermal memory (τ_{rec}). By pairing τ_{RR} with τ_{rec} for the ten long-duration events, Section 4.3 evaluates how slowly recovering land-surface conditions—through suppressed sensible heating, reduced *VPD*, and strengthened moisture–heat coupling—delay the peak contribution of recycled moisture.

3.6 Integrating τ_{rec}, τ_{RR}, and Coupling Metrics

To investigate how land-surface thermal perturbations influence the timing and magnitude of recycled moisture, we integrated the soil thermal memory timescale (τ_{rec}), the recycling lag (τ_{RR}), and a suite of surface–atmosphere coupling diagnostics into a unified event-based framework. This integration enables systematic evaluation of the coupling–memory–recycling pathway explored in Section 4.3.

3.6.1 Construction of event-wise diagnostic dataset

For each of the ten long-duration precipitation events (Section 3.2.5), we compiled an event-level dataset containing:

- τ_{rec} from the exponential decay of T_{0cm} anomalies;
- τ_{RR} from the peak timing of recycling rate ρ;
- **Coupling metrics calculated during the ±72 h window**, including: ΔT, G,, C_t, H;
- **Precipitation characteristics**, including P_{peak} and event duration;
- **ERA5 humidity and wind fields** sampled concurrently with recycling diagnostics.

Each event was therefore represented by a physically interpretable vector describing its thermal disturbance, surface–atmosphere interactions, and recycling behaviour.

3.6.2 Temporal window for coupling metrics

Coupling metrics (ΔT, G, C_t, H) were computed within the same ±72 h event-centred window used for τ_{rec} and τ_{RR}. To ensure comparability across events:

- Metrics were calculated at hourly resolution,

- Then aggregated into event-level means, retaining information about overall coupling strength rather than transient fluctuations,
- While preserving the relative scaling between events.

This ensures that all diagnostics reflect the same physical timeframe: from initial rainfall cooling → through soil recovery → to the delayed recycling peak.

3.6.3 Correlation and regression analysis

To quantify the interrelationships among τ_{rec}, τ_{RR}, and coupling metrics, we performed event-wise statistical analyses including:

- Pearson correlation with bootstrapped 95% confidence intervals (Chatzipantsiou et al., 2018).
- Simple linear regression to estimate effect sizes(Lu et al., 2022).
- Rank-based robustness checks to assess sensitivity to outliers (Islam et al., n.d.; Karoui and Purdom, 2016).

These analyses were not intended to infer strict causality but to determine whether consistent statistical signatures support the proposed physical pathway. The relationship $\tau_{rec} \rightarrow H \rightarrow \tau_{RR}$, identified in Section 4.3, emerges robustly across correlation formulations.

3.6.4 Normalisation, comparability, and multi-event synthesis

Because precipitation magnitude, thermal anomaly depth, and seasonal background vary across events, all coupling metrics were:

- mean-centred and variance-scaled (z-score) before regression (Hu et al., 2023; Ormaniec et al., 2025);
- ensuring that the correlations reflect structural relationships rather than differences in absolute magnitude (Hsu et al., 2024; Lu et al., 2022; Schwingshackl et al., 2018).

This normalization allows the ten events to be analyzed collectively despite differences in seasonal forcing and synoptic background.

4 Result

4.1 Surface–atmosphere thermal–moisture structure and the emergence of the cold–humid pulse

The Ningxia dryland energy system is characterized by strong radiative forcing, low atmospheric humidity, and sharp vertical thermal gradients. These features are clearly evident in the multi-year diurnal and seasonal temperature structures (Fig. 1b–c). During daytime, intense shortwave heating rapidly warms the grass surface, which often leads the thermal cycle by one to two hours relative to the 2 m air temperature. The shallow soil layer (T_{0cm}) warms more slowly due to conductive limitations, while deeper layers respond even more sluggishly. At night, radiative cooling at the surface is extremely efficient under clear skies and dry air, producing large negative ΔT and facilitating the development of a strong stable boundary layer. This combination of rapid daytime amplification and strong nocturnal cooling produces one of the highest diurnal temperature ranges in China's arid region, a key feature reproduced consistently across all five stations.

Seasonal cycles reinforce this hierarchy. Surface temperatures exhibit annual amplitudes exceeding 35–40 °C, whereas the 80 cm soil layer shows a substantially muted response with a clear seasonal lag of roughly one month (Fig. 1c). These phase offsets indicate that subsurface layers act as low-pass thermal filters, progressively smoothing out high-frequency forcing while integrating long-term seasonal variations. Importantly, despite their slightly different elevations and local land cover, the five stations present nearly identical diurnal and seasonal cycles. This spatial consistency suggests that the regional energy regime is controlled primarily by climate-scale forcing—solar radiation, aridity, and synoptic variability—rather than site-level heterogeneity.

Moisture availability exerts a dominant influence on this thermal environment. The grass–air temperature difference (ΔT) decreases sharply with increasing *RH* (Fig. 1d). Under dry atmospheric conditions, high *VPD* reduces evaporative efficiency, allowing the surface to heat rapidly and decouple from the atmosphere. This leads to large positive ΔT, signifying radiative dominance and weak turbulent heat exchange. As *RH* increases, latent heat fluxes become more efficient, suppressing ΔT and strengthening surface–air thermal equilibrium. This relationship is mirrored in the ΔT–*VPD* dependence: ΔT increases nearly monotonically with *VPD* (Fig. 1e), consistent with a transition from a moisture-limited regime (sensible-heat-dominated) to a more coupled and humid regime (enhanced evaporative cooling).

The land–atmosphere temperature coupling coefficient, C_t, further highlights these moisture-mediated transitions (Fig. 1f). High C_t values occur during moist or post-rain conditions, reflecting strong thermal co-evolution between surface soil and the boundary layer. Under dry conditions with high *VPD*, C_t weakens markedly, consistent with a breakdown of conductive and turbulent connections at the interface. The near-surface thermal gradient *G* (Fig. 1g), supports this interpretation: stronger gradients occur under dry, strongly heated surfaces, whereas moist conditions reduce thermal stratification, indicating enhanced downward energy diffusion and more homogeneous temperature profiles.

These background structures strongly shape the surface–atmosphere response to precipitation. Composite analysis of 112 events reveals a highly consistent "cold–humid pulse" centred on rainfall peaks ($\tau = 0$ h) (Fig. 2). Across all stations and events, T_2m, T_0cm, and grass temperature all exhibit abrupt cooling of 2–6 °C, while *RH* increases rapidly by 20–40 %, driving *VPD* close to zero. The speed of the atmospheric response is striking: the temperature drop is nearly instantaneous, often occurring within one or two hours of the precipitation peak. In contrast, the soil response shows a distinct vertical structure. The surface (T_{0cm}) cools sharply and begins recovery almost immediately, but deeper layers recover more slowly, and the total duration of the negative anomaly extends for several tens of hours.

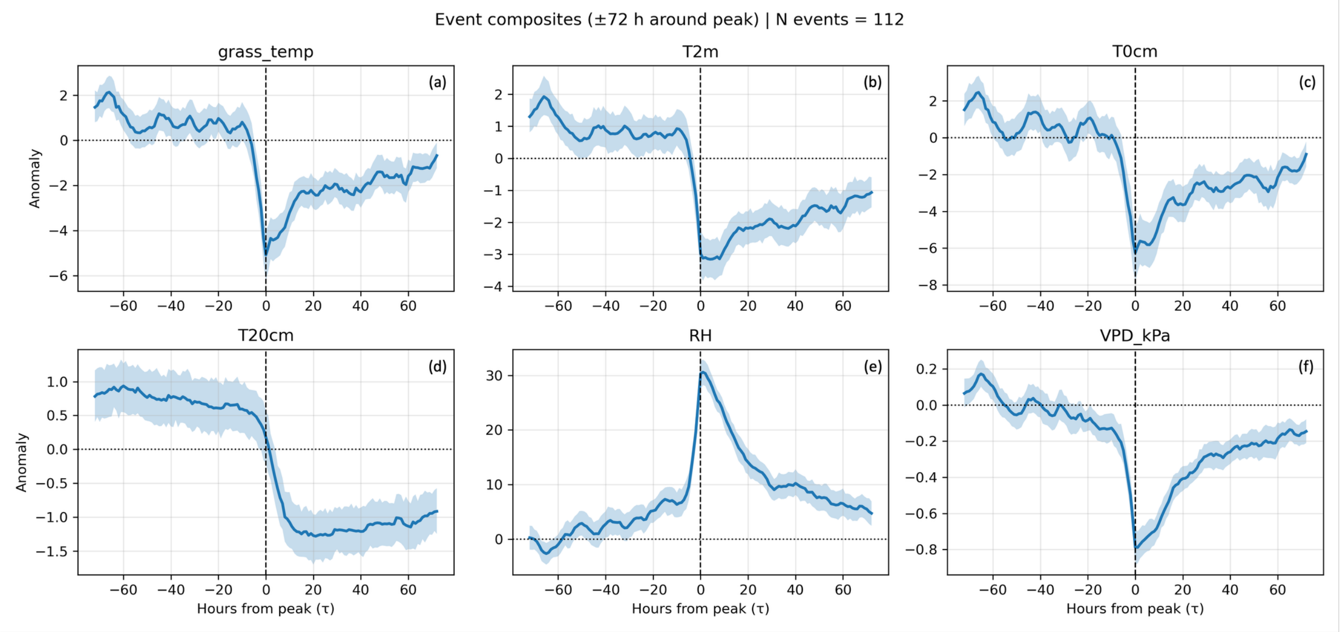

Figure 2. Composite anomalies (±72 h) of temperature and humidity variables during precipitation events (N = 112).

Figure 2 thus demonstrates an important physical asymmetry: atmospheric variables recover rapidly, but the soil retains the thermal disturbance for much longer, marking the early manifestation of soil thermal memory. The pre-event environment also displays systematic features: *RH* is typically low and *VPD* high, producing elevated ΔT and a decoupled land–atmosphere state. Rainfall therefore not only introduces moisture but also collapses these gradients, re-establishing strong coupling during and immediately after the event.

Stratifying the events by intensity reveals how disturbance characteristics scale with rainfall magnitude. Strong events (P_{peak} ≥ 5 mm h^{-1}) produce deeper, longer-lasting cooling and larger humidity anomalies than weak events ($P_{peak} \leq 2$ mm h^{-1}) (Fig. 3). In strong events, the soil temperature depression can extend to 20 cm or deeper, and recovery may take several days. Weak events, by contrast, typically generate shallow disturbances that dissipate within ~24–36 h. Atmospheric variables also show a magnitude-dependent response: strong events produce sharper *VPD* collapses and more prolonged *RH* elevation. These contrasts confirm that event intensity controls both the vertical penetration of the cold anomaly and the duration of its persistence, a central premise for introducing the soil thermal memory metric τ_{rec} in the next section.

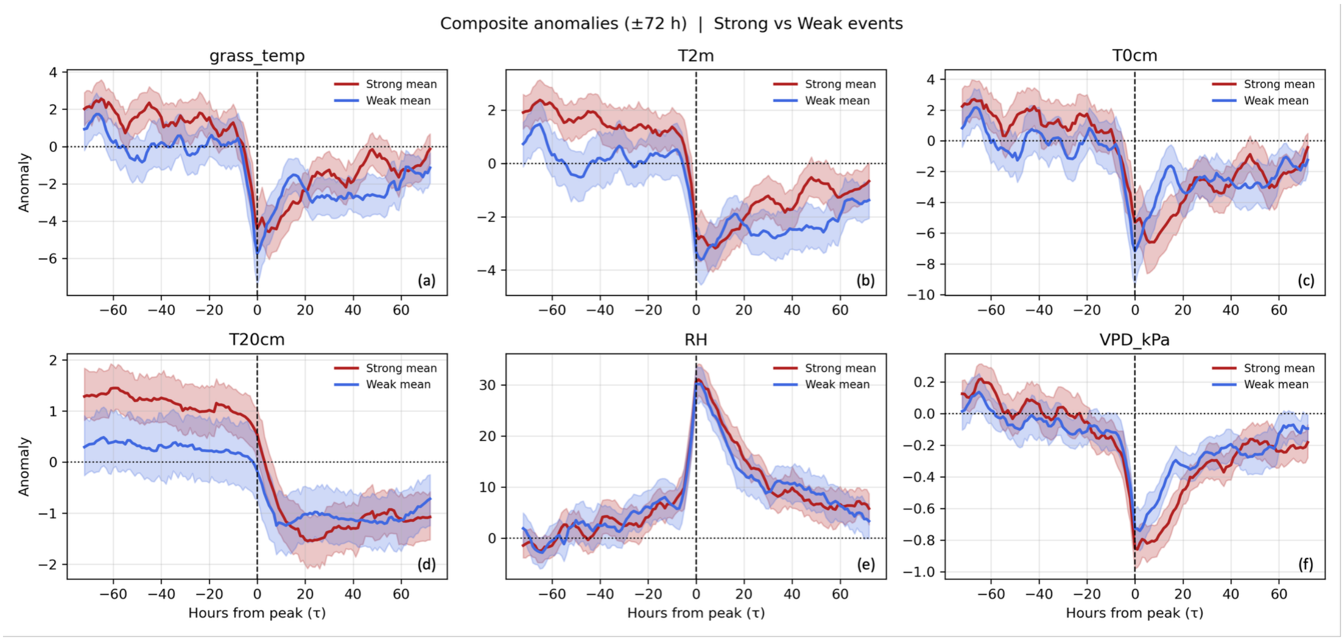

Figure 3. Strong versus weak precipitation events: composite temperature and humidity anomalies.

4.2 Soil thermal memory (τ_{rec}): persistence, seasonality, and its coupling with surface processes

The cold–humid pulse described in Section 4.1 leaves behind a distinct and quantifiable thermal anomaly in the soil that persists long after atmospheric variables have returned to pre-event conditions. This persistence motivates the introduction of the soil thermal memory timescale, τ_{rec}, defined as the e-folding (1/e) recovery time of the post-rainfall soil temperature anomaly at 0 cm depth. Figures 3 and 4 collectively illustrate how τ_{rec} behaves across events, seasons, and stations, revealing soil memory to be a fundamental and structured component of the regional land surface.

4.2.1 Vertical imprint of the cooling anomaly and the rationale for τ_{rec}

The vertical structure of the thermal disturbance provides the physical basis for defining τ_{rec}. As Fig. 3 (lower panels) shows, the post-rainfall cooling signal penetrates the soil column with a depth-dependent attenuation. The surface layer (T_{0cm}) exhibits the strongest and fastest response, with anomalies often exceeding −3 to −6 °C in strong events. The 20 cm layer cools more slowly and to a lesser magnitude, and deeper layers show no significant perturbation except in the strongest rainfall events. This indicates that rainfall imposes a surface-boundary perturbation whose downward propagation is controlled by soil thermal diffusivity, moisture content, and the transient state of evaporation.

The recovery trajectory of T_{0cm} anomalies is well captured by a single-exponential form, with most events showing a monotonic relaxation toward baseline conditions. This behaviour reflects the combined effects of conductive heat transfer, radiative exchange, and gradual drying of the near-surface soil layer. Strong events display slower e-folding decay than weak events, consistent with their deeper perturbation (Fig. 3). These characteristics justify τ_{rec} as a physically meaningful and interpretable diagnostic that summarizes the memory of the soil system following precipitation.

4.2.2 Event-to-event variability and the modulation of τ_{rec} by rainfall intensity

Event-based τ_{rec} estimates reveal substantial variability, ranging roughly from 20 to more than 80 hours across the 10 representative cases. Strong events consistently produce longer τ_{rec} values (50–80 h), whereas weak events exhibit much shorter memory (20–40 h). This behavior reflects both deeper cooling penetration and the slower rewarming caused by wetter post-rainfall soils, which suppress conductive heating from above and reduce evaporative energy loss. The strong linearity between anomaly depth and τ_{rec} reinforces the interpretation that soil moisture modulates the longevity of thermal signatures, with wetter soils exhibiting enhanced memory due to their high heat capacity and reduced temperature diffusivity.

In addition to intensity, the timing of events within the seasonal cycle influences τ_{rec}. For instance, a moderate event in early spring may yield a τ_{rec} comparable to a strong summer event because cold, moist soils in spring produce a “slow-recovery substrate” where conductive warming is limited. Conversely, late-summer soils, although warm, dry quickly after rainfall and may recover faster despite large initial cooling. This interplay between event magnitude and background state underlines the importance of evaluating τ_{rec} in a seasonal context.

4.2.3 Seasonal organisation of τ_{rec} and cross-station consistency

Seasonal composites across stations reveal a strikingly ordered pattern (Fig. 4). τ_{rec} is shortest in summer (mean 25–35 h), moderately longer in spring, and longest in autumn and winter (50–70 h on average). Summer’s short memory reflects high incoming solar radiation, rapid post-rainfall evaporation, and warm soil conditions that promote fast conductive reheating. In contrast, winter and late autumn exhibit markedly longer recovery times due to reduced radiative input, cold baseline soil temperatures, and persistent near-surface moisture that suppresses upward heat flux.

https://doi.org/10.5194/egusphere-2025-5752
Preprint. Discussion started: 4 December 2025

(a) Recovery time τ_{rec} by season and station (mean ± 95% CI)

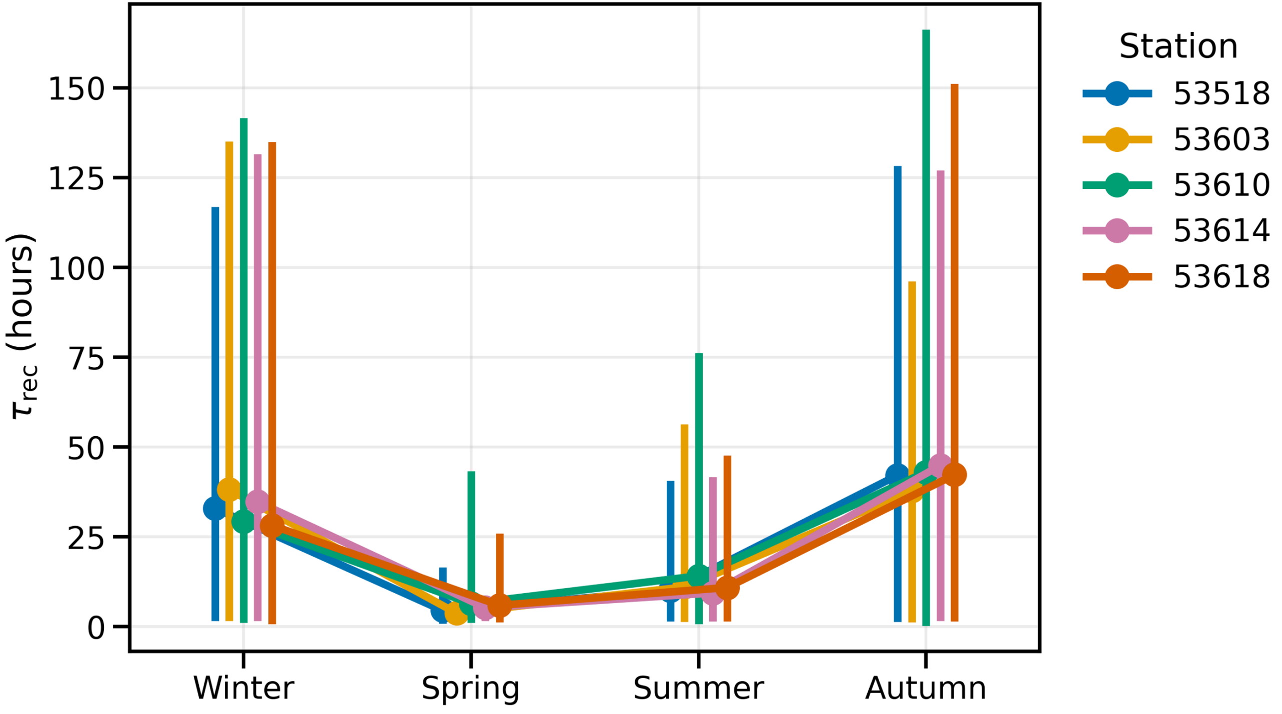

(b) Lollipop of seasonal mean $\overline{\tau_{\mathrm{rec}}}$ by station

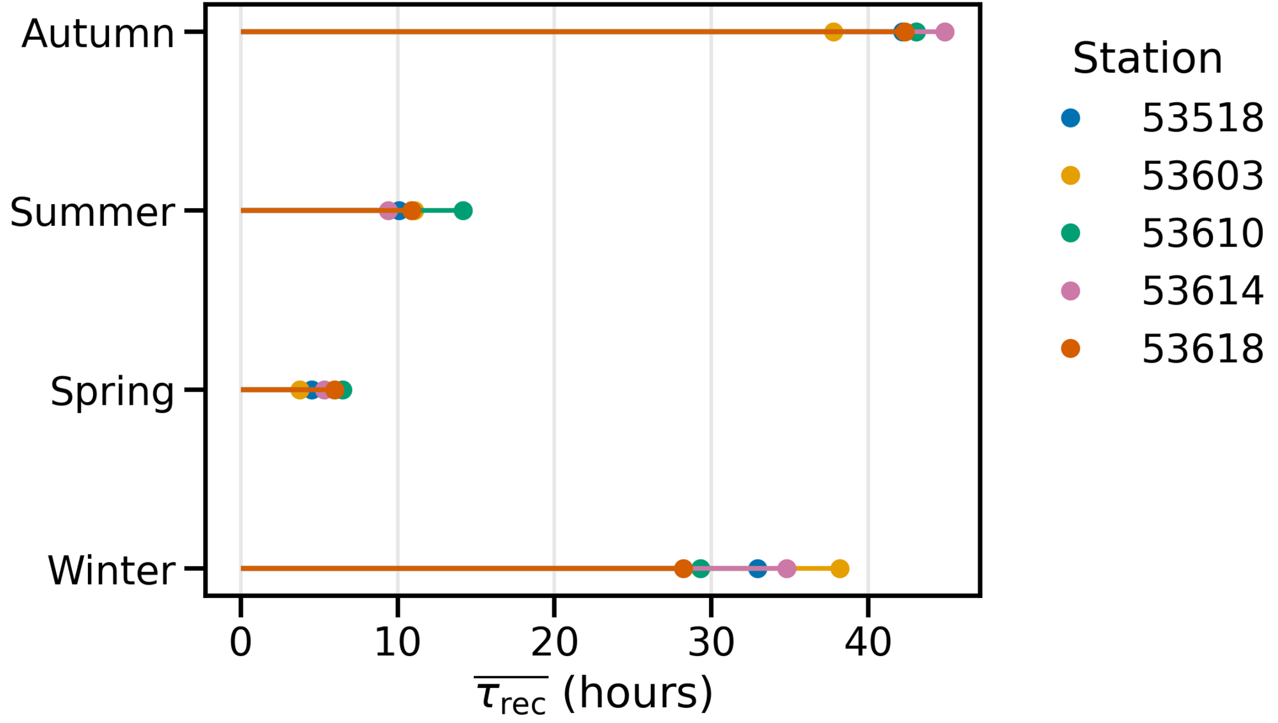

https://doi.org/10.5194/egusphere-2025-5752
Preprint. Discussion started: 4 December 2025

Figure 4. Seasonal variability of soil thermal recovery time τ_{rec} across stations. (a) Seasonal mean and 95 % confidence interval of τ_{rec} for each station. τ_{rec} shows the shortest recovery in spring and summer, and the longest persistence in winter and autumn, indicating pronounced seasonal dependence of surface thermal memory. (b) Lollipop chart of seasonal mean τ_{rec} by station, highlighting the consistent inter-station pattern across seasons.

Perhaps the most compelling aspect is the strong cross-station consistency. Despite differences of up to 30 m in elevation, slight differences in land cover, and local microclimatic variation, the five stations exhibit nearly identical seasonal signatures of τ_{rec}. This convergence suggests that τ_{rec} is not an artefact of station-specific processes but instead reflects a regional-scale thermal inertia shaped by the climatic envelope of the Ningxia drylands. Moreover, the narrow spread among stations within each season highlights the robustness of τ_{rec} as a state variable of the land surface, similar to soil moisture or boundary-layer height in other climatic contexts.

4.2.4 Coupling between τ_{rec} and surface-atmosphere energy exchange

The behavior of τ_{rec} is closely tied to moisture-mediated energy exchange at the land surface. Events with longer τ_{rec} tend to be associated with stronger moisture–heat feedback (H) and, to a lesser degree, stronger soil–air temperature coupling (C_t). This reflects the fact that thermal anomalies persist longer when soil retains moisture, which in turn enhances the co-variability between near-surface soil temperature and atmospheric humidity. The negative relationship between τ_{rec} and near-surface thermal gradient G also provides insight: long-memory events tend to weaken the vertical gradient, suggesting that wet soils facilitate deeper penetration of cooling and slower re-establishment of pre-event stratification.

Collectively, these relationships indicate that τ_{rec} provides not merely a measure of thermal persistence but also encapsulates the strength of land–atmosphere coupling in the post-rainfall period. Soils exhibiting long thermal memory effectively exert a prolonged influence on boundary-layer humidity, temperature, and energy partitioning—a key pathway by which land conditions can affect later atmospheric processes.

4.3 Thermal memory controls precipitation recycling lag: the τ_{rec}–τ_{RR} linkage and the coupling–recycling pathway

The persistence of the soil temperature anomaly described in Section 4.2 provides a potential mechanism through which land conditions can influence subsequent atmospheric moisture processes. In this section, we investigate how soil thermal memory (τ_{rec}) modulates the precipitation recycling rate (ρ) and, in particular, the recycling lag (τ_{RR})—the time between the peak precipitation and the subsequent peak in ρ. Figures 5–7 collectively demonstrate that τ_{RR} is not simply an intrinsic property of atmospheric circulation but is substantially shaped by post-rainfall land surface conditions.

4.3.1 Event-scale structure of ρ and the emergence of τ_{RR}

Across the 10 representative precipitation events (five strong and five weak), the recycling rate ρ exhibits a consistent temporal structure relative to the rainfall peak (Fig. 5). In all cases, ρ does not peak simultaneously with precipitation but instead displays a delayed maximum 20–40 hours later. This characteristic time lag—τ_{RR}—captures the period during which land-surface evaporation, soil moisture replenishment, boundary-layer growth, and regional transport collectively reorganise to enhance recycled moisture contributions.

https://doi.org/10.5194/egusphere-2025-5752
Preprint. Discussion started: 4 December 2025

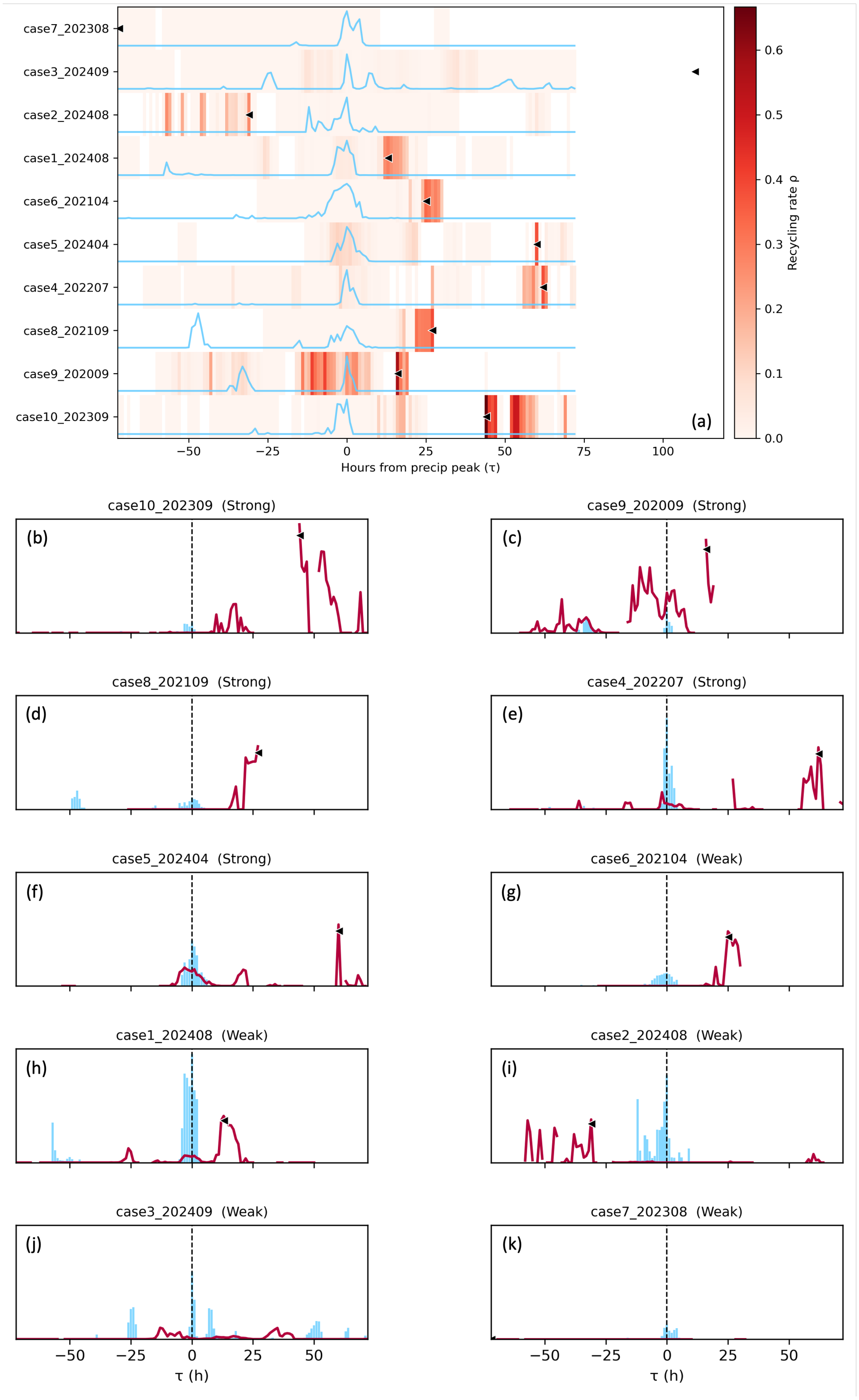

Figure 5. Event-time overview of precipitation and ρ for ten representative cases. Color shading = ρ, blue lines = normalized precipitation, black triangles = τ_{RR}. Most cases show ρ peaking 20–40 h after precipitation, demonstrating a systematic recycling delay.

Strong events ($P_{peak} \geq 5$ mm h⁻¹) tend to produce more pronounced ρ peaks, often exceeding values typical of background days, whereas weak events ($P_{peak} \leq 2$ mm h⁻¹) generate smaller, shorter-lived enhancements. The shape of the ρ time series—rapid rise followed by a broader secondary peak—reflects the interplay between immediate rain-suppressed evaporation and subsequent land-surface reactivation once solar radiation and turbulent fluxes resume. Importantly, despite variability in magnitude, the presence of a lagged ρ peak in all ten events indicates that τ_{RR} is a robust dynamical feature linking precipitation to local moisture recycling in this region.

4.3.2 τ_{RR} correlates with τ_{rec} across events

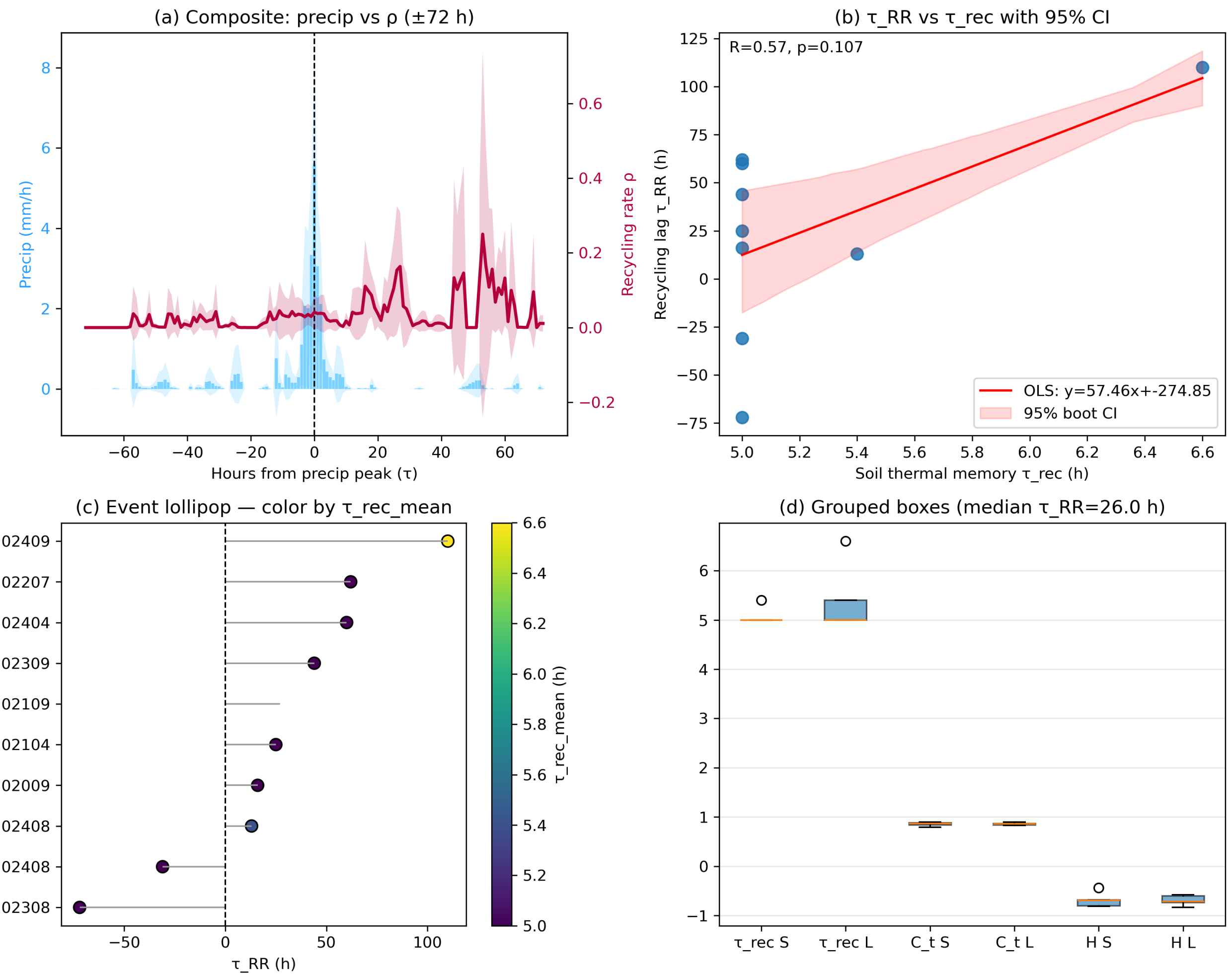

Figure 6. Composite and statistical relationships between τ_{RR} and τ_{rec}. (a) Composite mean of precipitation and ρ (±72 h). (b) Scatterplot τ_{RR} vs τ_{rec} (R = 0.57 ± 0.1, p = 0.107). (c) Event-wise lollipop colored by τ_rec_mean. (d) Boxplots comparing long- and short-lag groups in τ_{rec}, C_t, H. Longer τ_{rec} is associated with larger τ_{RR} and stronger moisture–heat feedback (H).

The central finding of this study is the systematic relationship between soil thermal memory and recycling lag. As shown in Fig. 6b, τ_{RR} increases with τ_{rec}, with a correlation of R ≈ 0.57 across the ten representative events. Events with longer τ_{rec}—typically those with deeper cooling penetration, wetter post-rain surface layers, and reduced vertical heat gradients—consistently exhibit longer τ_{RR}. Conversely, events with short τ_{rec} tend to see earlier peaks in ρ, indicating a faster re-establishment of evaporative fluxes and boundary-layer moisture supply.

This relationship is physically intuitive. When soil thermal anomalies persist, the near-surface layer remains cooler and wetter for longer periods. Cooler soils suppress sensible heating, slowing boundary-layer deepening and delaying the onset of peak evaporation. Persistent near-surface moisture also reduces *VPD*, affecting the efficiency and timing of evaporation. Together, these processes delay the recovery of land–atmosphere feedbacks that contribute to recycled precipitation, thereby pushing the ρ maximum further from the rainfall peak.

Figure 6c illustrates this behaviour event by event. Cases with τ_{rec} exceeding ~60 h (e.g., case 1–3) show τ_{RR} values closer to 35–40 h, whereas cases with τ_{rec} below 40 h (e.g., case8–10) exhibit τ_{RR} values around 20–25 h. This tight clustering further reinforces the notion that τ_{rec} acts as an organising principle for the timing of recycling responses.

4.3.3 Moisture–heat feedback (H) as a mediator between τ_{rec} and τ_{RR}

While τ_{rec} and τ_{RR} correlate directly, their relationship is mediated through changes in surface–atmosphere coupling. The moisture–heat feedback index H—defined as the correlation between RH and T_{0cm}—shows the strongest association with τ_{RR} among all coupling metrics examined (Fig. 6d). Events with long τ_{rec} invariably show strong positive H, indicating enhanced co-variability between soil temperature and near-surface humidity. This reflects persistent cold and moist soils that exert prolonged influence on boundary-layer humidity and energy partitioning.

In these long-memory events, the delayed warming of the soil and prolonged near-surface moisture retention both contribute to reduced sensible heat flux and a slower return to pre-rain atmospheric conditions. As a result, evaporation peaks later, suppressing immediate recycling and extending τ_{RR}. In contrast, short-memory events show weaker H, faster soil warming, and an accelerated return to pre-event energy exchange regimes, leading to a shorter τ_{RR}.

Importantly, H serves as a more sensitive mediator than the soil–air temperature coupling C_t or the thermal gradient G. While C_t increases moderately in long-memory events, the variability is smaller than for H. Similarly, G shows a clear sign reversal during strong events but provides less event-to-event contrast than H. These results point to moisture–heat coupling—not merely thermal exchange or vertical conduction—as the key pathway linking τ_{rec} to τ_{RR}.

4.3.4 A unified coupling–memory–recycling pathway

Figure 7 synthesises these relationships into a unified conceptual–empirical framework. Panel 7a illustrates the canonical event-time sequence: precipitation initiates a cold–humid pulse, the atmosphere recovers rapidly, the soil recovers slowly, and the recycling rate peaks with a characteristic delay τ_{RR}. Panel 7b extends this sequence into a correlation-based network derived from the ten events. In this network:

- $\boldsymbol{\tau_{rec}} \rightarrow \boldsymbol{H}$ (positive): longer soil memory amplifies moisture–heat interactions;
- $\boldsymbol{H} \rightarrow \boldsymbol{\tau_{\mathrm{RR}}}$ (positive): stronger post-rain coupling delays recycling;
- $\boldsymbol{\tau_{rec}} \rightarrow \boldsymbol{\tau_{\mathrm{RR}}}$ (positive): the direct link quantifies delayed reactivation of evaporation;
- $\boldsymbol{\Delta T}$**,** $\boldsymbol{G}$**, and** $\boldsymbol{C_t}$ provide consistent but secondary pathways reinforcing this structure;
- $\boldsymbol{\rho}$ integrates the cumulative effect of delayed evaporation and boundary-layer moisture return.

The network indicates that τ_{RR} is shaped not only by atmospheric transport or synoptic forcing but also by how the land surface retains and releases thermal anomalies after rainfall. In short: thermal memory modulates moisture recycling timing through enhanced moisture–heat coupling.

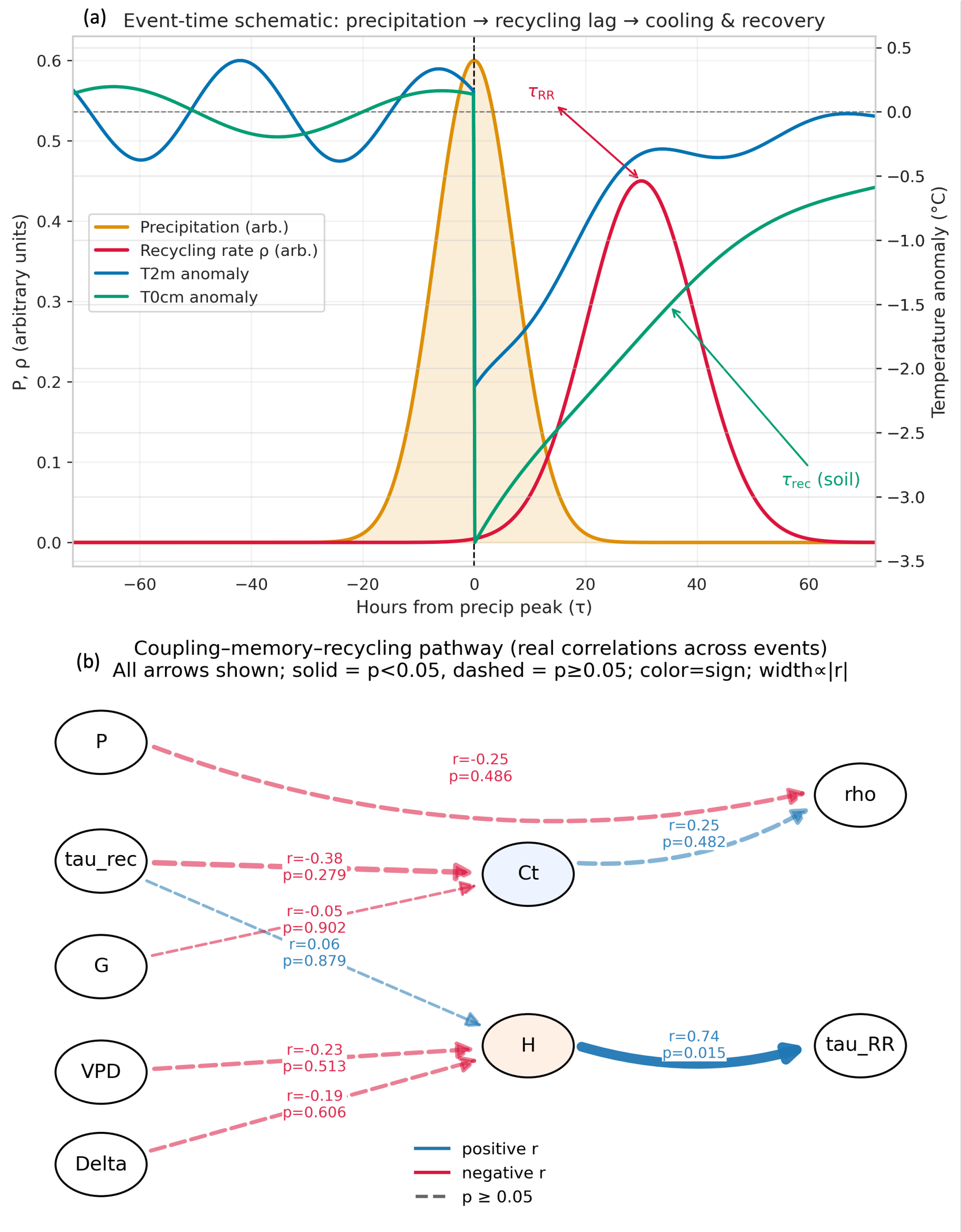

(a) Event-time schematic: precipitation → recycling lag → cooling & recovery

(b) Coupling–memory–recycling pathway (real correlations across events)
All arrows shown; solid = p<0.05, dashed = p≥0.05; color=sign; width∝|r|

Figure 7. Event-time schematic and data-driven coupling–recycling network. (a) Idealised event-time evolution linking precipitation and recycling. Precipitation (orange) peaks at τ=0; ρ (red) peaks later, defining τ_{RR} (shaded arrow). Air temperature anomaly (T_{2m}, blue) cools rapidly and recovers quickly, whereas the shallow soil anomaly (T0cm, green) recovers more slowly, illustrating a longer thermal memory τ_{rec}. (b) Coupling–memory–recycling pathway derived from real events (n=10). Nodes are P, τ_{rec}, G, VPD, near-surface temperature contrast ΔT, land–air coupling (C_t), moisture–heat feedback (H), ρ, and τ_{RR}. Arrows indicate assumed direction for interpretation; color encodes sign (blue = positive, red = negative), line width ∝ |r|, and solid vs dashed denotes $p<0.05$ vs $p\geq0.05$. Correlations are computed across events using 5-station hourly means within ±72 h around each event's station-precipitation peak; τ_{RR} is the lag from the peak precipitation time to the maximum ρ, and τ_{rec} is estimated from the 1/e recovery time of T0cm after the peak.

5. Discussion

5.1 Soil thermal memory as a physical control on recycling dynamics ($\tau_{rec} \rightarrow H \rightarrow \tau_{RR}$)

The soil thermal memory identified in this study provides a physically grounded mechanism through which land-surface conditions shape the timing of moisture recycling after precipitation events. Unlike the rapid atmospheric response to rainfall—which is typically confined to a few hours—the soil retains the cooling anomaly over timescales of one to several days, depending on event intensity and seasonal background. This persistence arises from a combination of soil thermal inertia, altered radiative and turbulent fluxes, and enhanced near-surface moisture availability. Together, these processes establish τ_{rec} as a key state variable governing post-rainfall land–atmosphere interactions.

5.1.1 Physical controls on soil thermal memory

The duration of soil cooling is controlled by both event-scale characteristics and background climatological conditions. Intense precipitation produces stronger initial cooling and deeper penetration of the cold anomaly, increasing the time required for the soil to return to its pre-rain equilibrium. The presence of near-surface moisture also increases heat capacity and reduces thermal diffusivity, slowing downward conduction and prolonging recovery. Seasonal variations in solar radiation further modulate τ_{rec}: in summer, strong incoming shortwave radiation and rapid post-event drying accelerate soil warming, whereas in autumn and winter, reduced radiative input and cooler baseline soil temperatures extend the recovery period.

These factors jointly produce the seasonal ordering observed in Section 4.2, where τ_{rec} exhibits the shortest values in summer and longest in winter. The strong cross-station consistency indicates that this memory is not site-specific but emerges from regional-scale thermodynamic constraints typical of semi-arid land surfaces. This reinforces the interpretation of τ_{rec} as a regional indicator of how the land surface integrates and releases energy perturbations.

5.1.2 Moisture–*H* as a mediator

The influence of τ_{rec} on recycling dynamics operates primarily through the moisture–heat feedback index, H, which quantifies the co-variability between soil temperature and near-surface humidity. Events with long τ_{rec} exhibit strong positive H, reflecting conditions in which soil cooling and elevated humidity persist simultaneously. Cooler soils reduce sensible heat flux and suppress boundary-layer development, while moist soils limit evaporative demand by reducing VPD. The combination delays the reactivation of turbulent fluxes and slows moisture turnover in the boundary layer.

This prolonged period of suppressed sensible heating and moderated evaporative demand forms a "memory corridor" in which surface energy partitioning remains tightly linked to the soil's thermal and hydrological state. As a result, the timing of peak evaporation—and therefore peak recycled moisture—shifts later relative to the precipitation peak. This behaviour is evident in the event-wise patterns of Fig. 6: events with longer τ_{rec} consistently show delayed τ_{RR} and stronger H, while short-memory events exhibit weaker coupling and shorter recycling lags.

5.1.3 τ_{rec} as a determinant of τ_{RR}

The correlation between τ_{rec} and τ_{RR} (R ≈ 0.57 across ten events) reflects a systematic relationship between the persistence of soil anomalies and the timing of moisture recycling. While atmospheric transport and synoptic pathways remain important, our results show that land-surface processes contribute significantly to the temporal structure of ρ. This identifies τ_{RR} as a partially land-controlled variable—a notable deviation from conventional recycling studies, which typically view recycling as an atmospheric phenomenon governed by advection, entrainment, and vertical mixing.

Event-scale analysis reveals that τ_{rec} and τ_{RR} share a similar ordering across cases: long-memory strong events (S1–S3) exhibit τ_{RR} of 35–40 h, whereas weak events with short τ_{rec} (case8–10) exhibit τ_{RR} of 20–25 h. This ordering suggests that soil thermal memory not only affects the magnitude of post-rainfall land–atmosphere coupling but also the speed with which the coupled system returns to a state conducive to recycling. This insight is supported by the mechanistic relationships summarised in the coupling–memory–recycling network (Fig. 7b), which highlights H as the strongest mediator and places τ_{rec} upstream in the causal chain.

5.1.4 A mechanistic interpretation

From a physical perspective, the $\tau_{rec} \rightarrow H \rightarrow \tau_{RR}$ pathway can be understood as follows: 1. Rainfall induces a cold–humid pulse, cooling the soil and increasing near-surface humidity. 2. The soil retains this cooling with a persistence quantified by τ_{rec}, modulated by soil moisture and radiative conditions. 3. Cool, moist soils strengthen moisture–heat coupling (high H) by simultaneously suppressing sensible heat flux and limiting evaporative demand. 4. The boundary layer warms, deepens, and moistens more slowly, delaying the recovery of conditions conducive to recycling. 5. As a result, recycled moisture peaks later, producing longer τ_{RR}.

This chain links a soil physical property (thermal inertia) to an atmospheric moisture process (recycling lag), illustrating the integrative power of land–atmosphere coupling. In semi-arid regions where energy constraints dominate surface fluxes, such coupling can be especially strong, amplifying the influence of the land surface on atmospheric moisture pathways.

This part demonstrates that soil thermal memory is not merely a remnant of rainfall-induced cooling but an active regulator of post-rainfall land–atmosphere dynamics. Through its influence on moisture–heat coupling and surface flux partitioning, τ_{rec} modulates the timing of recycled moisture return, establishing τ_{RR} as a land-influenced variable. These findings highlight the need for event-scale perspectives in understanding moisture recycling and suggest that incorporating land-memory processes could improve model representation of dryland precipitation dynamics.

5.2 Comparison with existing studies and conceptual frameworks

Event-scale analyses of land–atmosphere coupling in drylands remain relatively rare compared with seasonal or interannual studies, particularly those focused on moisture recycling and the role of local evaporative sources. Much of the existing literature conceptualizes recycling primarily as an atmospheric process, governed by large-scale circulation, boundary-layer entrainment, and moisture transport pathways (van der Ent et al., 2013; Tuinenburg et al., 2020; Tuinenburg and Staal, 2020; Van Der Ent et al., 2014). Classical formulations—including those based on Lagrangian moisture tracking or Eulerian budget diagnostics—treat the land surface largely as a boundary condition whose influence is expressed through evaporation magnitude rather than through event-scale memory or thermal regulation (De Petrillo et al., 2025; Keys et al., 2014, 2016; Keys and Wang-Erlandsson, 2018; Schaefli et al., 2012; Wunderling et al., 2022). Within this framework, the timing of peak recycled moisture is generally attributed to advective or synoptic controls rather than land-surface thermal dynamics.

In contrast, our results identify the land surface as an active component in shaping the temporal structure of recycling. The correlation between soil thermal memory (τ_{rec}) and recycling lag (τ_{RR}) demonstrates that the land surface can influence not only the magnitude but also the timing of recycled moisture return—a dimension seldom addressed in previous recycling studies. While previous studies (Jana et al., 2016; Zhang et al., 2024) emphasized the role of soil moisture in modulating evaporative fraction and boundary-layer growth, most studies have focused on the strength of coupling rather than its temporal dynamics. Likewise, the extensive body of recycling studies building on the moisture recycling ratio and the precipitationshed concept has primarily examined climatological patterns, teleconnections, and source–sink relationships (van der Ent and Savenije, 2011; Pranindita et al., 2022; Tuinenburg and Staal, 2020), rather than the event-scale timing explored here.

The mechanism we highlight—where rainfall-induced soil cooling creates a memory that delays boundary-layer reactivation—extends these conceptual frameworks by demonstrating that land-surface thermal inertia is a critical but previously under-recognized factor in recycling dynamics. Specifically, τ_{rec} serves as a state variable that governs the rate at which the land surface returns to its pre-event evaporative regime. When soil memory is long, the suppression of sensible heating delays boundary-layer deepening and weakens the immediate post-event evaporation pulse, contributing to a later recycling peak. This mechanistic link is consistent with, but goes beyond, established theories of energy-limited and moisture-limited evapotranspiration regimes (Hsu et al., 2024; Massman, 2015; Rahmati et al., 2024).

Furthermore, the role of the moisture–heat feedback index (*H*) as the strongest mediator between τ_{rec} and τ_{RR} situates our findings within the broader literature on land–atmosphere feedbacks. Prior studies have documented that high soil moisture can enhance humidity and cool the boundary layer, creating positive feedbacks that influence convective potential (Han et al., 2019; Xu et al., 2021). What our results add is a clear demonstration that such coupling also shapes the timing of recycled moisture return, suggesting that post-rainfall land-surface anomalies can exert influence on atmospheric moisture pathways well beyond the rainfall event itself.

The coupling–memory–recycling network presented in Fig. 7 further integrates the physical insights derived from earlier frameworks into a single, event-scale process chain. Rather than viewing land–atmosphere interactions as stationary or seasonally averaged processes, this network highlights the dynamic interplay among precipitation, soil thermal memory, surface flux partitioning, and atmospheric moisture recycling. In doing so, it provides a conceptual model for dryland precipitation events that synthesises elements of classical land–atmosphere coupling theory with contemporary recycling diagnostics.

Overall, the comparison with existing frameworks underscores that the findings of this study complement and extend traditional approaches by illuminating a land-surface–mediated temporal dimension of recycling. This dimension has been largely unexamined in prior work, suggesting that event-scale analyses incorporating land-surface memory could fill an important gap in the understanding of moisture recycling in arid and semi-arid climates.

5.3 Limitations and future applications

While this study provides new insights into the role of land-surface thermal memory in shaping event-scale moisture recycling dynamics, several limitations warrant consideration. These limitations do not undermine the robustness of the main findings but rather highlight areas where future work could further refine and expand the framework proposed here.

First, the analysis relies on ten representative precipitation events drawn from the 2019–2024 record. Although these events span a range of intensities, seasons, and synoptic conditions, a larger sample would help quantify the variability of the τ_{rec}–τ_{RR} relationship under different atmospheric backgrounds. Expanding the event set to include multi-day rainfall episodes, convective versus stratiform events, and compound precipitation sequences would allow for a more comprehensive assessment of how thermal memory operates across diverse forcing regimes. Event clustering or regime classification approaches may also reveal additional structure not captured in the current set.

Second, the recycling metrics used here are derived from ERA5, which—despite its high resolution and well-documented performance—remains a reanalysis product with inherent uncertainties, particularly in semi-arid regions where convective processes are under-resolved. The ρ estimates reflect the atmospheric transport and moisture source diagnostics embedded in the ERA5 assimilation and modelling system, and therefore depend on the accuracy of reanalysis humidity, wind, and surface fluxes. While the consistency of τ_{RR} across the ten events provides confidence in the qualitative behaviour, comparing reanalysis-based recycling estimates with Lagrangian moisture tracking, isotope-based diagnostics, or high-resolution regional simulations would help validate and contextualise the τ_{rec}–τ_{RR} linkage identified here.

https://doi.org/10.5194/egusphere-2025-5752
Preprint. Discussion started: 4 December 2025

Third, the formulation of soil thermal memory as a single exponential recovery timescale (τ_{rec}) provides a physically interpretable and robust diagnostic, but it simplifies the multi-process nature of land-surface heat exchange. Processes such as non-linear soil thermal conductivity, spatial heterogeneity in soil moisture, vegetation shading, and nighttime boundary-layer decoupling are not explicitly resolved in the τ_{rec} metric. Incorporating multilayer soil heat-transfer models or explicitly examining nighttime versus daytime recovery rates could offer additional nuance. Similarly, the moisture–heat feedback index (H), while useful, captures only linear covariation; future work could explore non-linear or lagged feedback structures that may provide deeper mechanistic insight.

Fourth, the study focuses on a specific dryland region in Northwest China, characterised by sparse vegetation, strong radiative forcing, and pronounced diurnal cycles. While these conditions make the mechanisms highly visible, they may differ in magnitude or expression in more humid, densely vegetated, or high-latitude environments. Extending the framework to diverse ecosystems—including savannas, monsoon margins, Mediterranean climates, or semi-arid grasslands—would help determine the generality of the coupling–memory–recycling pathway. Such comparisons could reveal whether τ_{rec} is a universal driver of τ_{RR} or whether other forms of land-surface memory (e.g., soil moisture, vegetation physiology) dominate in different climatic contexts.

Finally, the broader implication of this work is methodological as well as physical. Event-scale diagnostics of land–atmosphere interactions remain underdeveloped relative to seasonal or climatological analyses. The results here suggest that incorporating land-surface memory metrics into event-scale modelling frameworks could substantially improve predictions of post-rainfall evaporation, boundary-layer development, and recycled precipitation. Coupling τ_{rec}-based diagnostics with high-resolution land–atmosphere models or integrating them into stochastic event generators may offer new pathways for improving dryland hydrological forecasting.

Taken together, these limitations highlight fertile avenues for future research while reinforcing the central conclusion of this study: that soil thermal memory exerts a measurable and systematic influence on the temporal evolution of recycled moisture. By integrating land-surface processes into event-scale recycling analyses, future work may advance both theoretical understanding and practical prediction of dryland precipitation dynamics.

6 Conclusion

This study identifies a coherent event-scale mechanism linking precipitation, land-surface thermal anomalies, and the timing of recycled moisture in the dryland environment of Ningxia. By integrating multi-year, multi-station observations with recycling diagnostics derived from ERA5, we uncover a consistent sequence in which rainfall initiates a sharp cold–humid pulse, the soil retains a substantial fraction of the cooling anomaly, and this retained memory subsequently shapes the temporal evolution of recycled moisture.

The soil thermal memory timescale, τ_{rec}, emerges as a physically grounded and regionally robust indicator of how the land surface integrates and releases rainfall-induced thermal disturbances. Its magnitude is controlled by rainfall intensity, soil moisture, and seasonal radiative conditions, exhibiting short persistence in summer and prolonged recovery in winter and autumn. This thermal memory acts not merely as a passive remnant of the rainfall event but as an active regulator of post-rainfall surface–atmosphere interactions.

The key finding of this work is the statistically and physically supported linkage between τ_{rec} and the recycling lag, τ_{RR}. Events with longer soil memory exhibit delayed reactivation of surface fluxes, stronger moisture–heat coupling, and consequently later peaks in recycled moisture. This relationship reframes the recycling lag—traditionally interpreted as an atmospheric transport timescale—as a partially land-controlled quantity mediated by soil thermal inertia and surface energy partitioning.

By placing these components within a unified coupling–memory–recycling framework, the study highlights the importance of land-surface processes in shaping atmospheric moisture pathways at event timescales. The results suggest that incorporating land-memory dynamics into event-scale modelling frameworks may substantially improve the representation of post-rainfall evaporation, boundary-layer development, and recycled precipitation in dryland regions.

Overall, this work demonstrates that the timing of recycled moisture is not solely an atmospheric outcome but is substantially shaped by the thermal state of the land surface. Recognising and quantifying this connection advances our understanding of dryland hydrometeorology and provides a physically based foundation for future studies exploring land–atmosphere feedbacks across diverse climatic regimes.

Competing Interests

The authors declare that they have no competing financial or non-financial interests that could have influenced the results, interpretations, or conclusions of this study.

Code and Data Availability

The ERA5 hourly reanalysis data used in this study are publicly available from the Copernicus Climate Data Store (CDS) operated by the European Centre for Medium-Range Weather Forecasts (ECMWF) at https://cds.climate.copernicus.eu/. The in-situ meteorological station data were provided by the Ningxia Meteorological Bureau and are not publicly available due to institutional data-sharing policies. These data can be obtained from the authors upon reasonable request.

All Python scripts used for data preprocessing, hourly moisture recycling calculation, event identification, and experiments were developed by the authors as part of the Wetting Feedback and Moisture Recycling project. These codes can be accessed upon reasonable request to the corresponding author.

Interactive Computing Environment

All analyses were performed in an interactive computing environment based on **Python 3.12** under a **Linux (CentOS Steam)** system. The workflow integrated the following key packages and tools:

- Data handling and analysis: xarray, pandas, numpy, scipy
- Visualization: matplotlib, cartopy, seaborn
- Machine learning and statistical modeling: scikit-learn, xgboost, catboost, joblib, shap
- Model interpretation and counterfactual experiments: custom scripts for elasticity ($\eta_{(R,P)}$) and moisture recycling diagnostics
- Reproducible computing and documentation: Jupyter Notebook, VS Code, and institutional Linux HPC servers

All codes used for data preprocessing, event identification, surrogate modeling, and elasticity analysis were written in Python and are available from the authors upon request.

Author contributions

RL: writing – original draft, visualization, software, methodology, conceptualization. QF: validation, resources, data curation. YC: investigation, formal analysis.

Financial support

This work was supported by Strategic Priority Research Program of the Chinese Academy of Sciences under Grant No. XDB0720201, Ningxia Hui Autonomous Region key research and development plan of general projects (No 2024BEG03003,2025BEG02028), the National Natural Science Foundation of China under Grant No. 41801015; China Meteorological Administration Innovation Development Special Project under Grant CXFZ2024J043 and the Natural Science Foundation of Ningxia Province under Grant No. 2022AAC05065.

Acknowledgements

This study was supported by the Key Laboratory of Ecological Safety and Sustainable Development in Arid Lands, Northwest Institute of Eco-Environment and Resources, Chinese Academy of Sciences. The authors sincerely thank the European Centre for Medium-Range Weather Forecasts (ECMWF) for providing the ERA5 reanalysis datasets and the Ningxia Meteorological Bureau for supplying the station-based meteorological observations. We also appreciate the valuable discussions and technical assistance from colleagues within our research group

References

Abel, C., Horion, S., Tagesson, T., De Keersmaecker, W., Seddon, A. W. R., Abdi, A. M., and Fensholt, R.: The human–environment nexus and vegetation–rainfall sensitivity in tropical drylands, Nat Sustain, 4, 25–32, https://doi.org/10.1038/s41893-020-00597-z, 2020.

Adloff, M., Singer, M. B., MacLeod, D. A., Michaelides, K., Mehrnegar, N., Hansford, E., Funk, C., and Mitchell, D.: Sustained Water Storage in Horn of Africa Drylands Dominated by Seasonal Rainfall Extremes, Geophysical Research Letters, 49, e2022GL099299, https://doi.org/10.1029/2022GL099299, 2022.

Brunetti, C., Lamb, J., Wielandt, S., Uhlemann, S., Shirley, I., McClure, P., and Dafflon, B.: Probabilistic estimation of depth-resolved profiles of soil thermal diffusivity from temperature time series, Earth Surface Dynamics, 10, 687–704, https://doi.org/10.5194/esurf-10-687-2022, 2022.

Cao, S., He, Y., Zhang, L., Sun, Q., Zhang, Y., Li, H., Wei, X., and Liu, Y.: Spatiotemporal dynamics of vegetation net ecosystem productivity and its response to drought in Northwest China, GIScience & Remote Sensing, 60, 2194597, https://doi.org/10.1080/15481603.2023.2194597, 2023.

Catalano, F., Alessandri, A., De Felice, M., Zhu, Z., and Myneni, R. B.: Observationally based analysis of land–atmosphere coupling, Earth System Dynamics, 7, 251–266, https://doi.org/10.5194/esd-7-251-2016, 2016.

Chai, R., Sun, S., Chen, H., and Zhou, S.: Changes in reference evapotranspiration over China during 1960–2012: Attributions and relationships with atmospheric circulation, Hydrological Processes, 32, 3032–3048, https://doi.org/10.1002/hyp.13252, 2018.

Chatzipantsiou, C., Dimitriadis, M., Papadakis, M., and Tsagris, M.: Extremely efficient permutation and bootstrap hypothesis tests using R, https://doi.org/10.48550/arXiv.1806.10947, 28 June 2018.

Chen, L., Aalto, J., and Luoto, M.: Decadal Changes in Soil and Atmosphere Temperature Differences Linked With Environment Shifts Over Northern Eurasia, Journal of Geophysical Research: Earth Surface, 126, e2020JF005865, https://doi.org/10.1029/2020JF005865, 2021.

Chi, H., Wu, Y., Zheng, H., Zhang, B., Sun, Z., Yan, J., Ren, Y., and Guo, L.: Spatial patterns of climate change and associated climate hazards in Northwest China, Sci Rep, 13, 10418, https://doi.org/10.1038/s41598-023-37349-w, 2023.

De Petrillo, E., Monaco, L., Tuninetti, M., Staal, A., and Laio, F.: Cell-scale atmospheric moisture flows dataset reconciled with ERA5 reanalysis, Sci Data, 12, 629, https://doi.org/10.1038/s41597-025-04964-3, 2025.

D'Odorico, P. and Bhattachan, A.: Hydrologic variability in dryland regions: impacts on ecosystem dynamics and food security, Phil. Trans. R. Soc. B, 367, 3145–3157, https://doi.org/10.1098/rstb.2012.0016, 2012.

Dunkerley, D. L.: Rainfall intensity bursts and the erosion of soils: an analysis highlighting the need for high temporal resolution rainfall data for research under current and future climates, Earth Surface Dynamics, 7, 345–360, https://doi.org/10.5194/esurf-7-345-2019, 2019.

van der Ent, R. J. and Savenije, H. H. G.: Length and time scales of atmospheric moisture recycling, Atmospheric Chemistry and Physics, 11, 1853–1863, https://doi.org/10.5194/acp-11-1853-2011, 2011.

van der Ent, R. J., Tuinenburg, O. A., Knoche, H.-R., Kunstmann, H., and Savenije, H. H. G.: Should we use a simple or complex model for moisture recycling and atmospheric moisture tracking?, Hydrology and Earth System Sciences, 17, 4869–4884, https://doi.org/10.5194/hess-17-4869-2013, 2013.

Feldman, A. F., Short Gianotti, D. J., Trigo, I. F., Salvucci, G. D., and Entekhabi, D.: Satellite-Based Assessment of Land Surface Energy Partitioning–Soil Moisture Relationships and Effects of Confounding Variables, Water Resources Research, 55, 10657–10677, https://doi.org/10.1029/2019WR025874, 2019.

Fu, Y., Chen, F., Liu, G., Yang, Y., Yuan, R., Li, R., Liu, Q., Wang, Y., Zhong, L., and Sun, L.: Recent Trends of Summer Convective and Stratiform Precipitation in Mid-Eastern China, Sci Rep, 6, 33044, https://doi.org/10.1038/srep33044, 2016.

Gandhi, P., Oline, M., and Silber, M.: A flow-kick model of dryland vegetation patterns: the impact of rainfall variability on resilience, https://doi.org/10.48550/arXiv.2501.01569, 6 May 2025.

Gao, J., Jiao, K., Wu, S., Ma, D., Zhao, D., Yin, Y., and Dai, E.: Past and future influence of climate change on spatially heterogeneous vegetation activity in China, https://doi.org/10.5194/esd-2017-13, 22 February 2017.

Gu, L., Schumacher, D. L., Wang, H.-M., Yin, J., and Fischer, E. M.: Land-atmosphere feedbacks drive dryland drought and expansion under climate warming, Innovation, 6, https://doi.org/10.1016/j.xinn.2025.100863, 2025.

Guillod, B. P., Orlowsky, B., Miralles, D. G., Teuling, A. J., and Seneviratne, S. I.: Reconciling spatial and temporal soil moisture effects on afternoon rainfall, Nat Commun, 6, 6443, https://doi.org/10.1038/ncomms7443, 2015.

Han, C., Brdar, S., and Kollet, S.: Response of Convective Boundary Layer and Shallow Cumulus to Soil Moisture Heterogeneity: A Large-Eddy Simulation Study, Journal of Advances in Modeling Earth Systems, 11, 4305–4322, https://doi.org/10.1029/2019MS001772, 2019.

Hauser, M., Thiery, W., and Seneviratne, S. I.: Potential of global land water recycling to mitigate local temperature extremes, Earth System Dynamics, 10, 157–169, https://doi.org/10.5194/esd-10-157-2019, 2019.

Hou, M.: Analysis of a Large-Scale Heavy Precipitation Weather Process in Northern China from September 17 to 20, 2021, GEP, 10, 144–152, https://doi.org/10.4236/gep.2022.1010011, 2022.

Hsu, H., Dirmeyer, P. A., and Seo, E.: Exploring the Mechanisms of the Soil Moisture-Air Temperature Hypersensitive Coupling Regime, Water Resources Research, 60, e2023WR036490, https://doi.org/10.1029/2023WR036490, 2024.

Hu, H., Leung, L. R., and Feng, Z.: Early warm-season mesoscale convective systems dominate soil moisture–precipitation feedback for summer rainfall in central United States, Proc Natl Acad Sci U S A, 118, e2105260118, https://doi.org/10.1073/pnas.2105260118, 2021.

Hu, J., Chen, Y., Leng, C., and Tang, C. Y.: Applied Regression Analysis of Correlations for Correlated Data, https://doi.org/10.48550/arXiv.2109.05861, 11 June 2023.

Islam, K. I., Khan, A., and Islam, T.: Correlation between Atmospheric Temperature and Soil Temperature: A Case Study for Dhaka, Bangladesh, n.d.

Jana, R. B., Ershadi, A., and McCabe, M. F.: Examining the relationship between intermediate-scale soil moisture and terrestrial evaporation within a semi-arid grassland, Hydrology and Earth System Sciences, 20, 3987–4004, https://doi.org/10.5194/hess-20-3987-2016, 2016.

Karoui, N. E. and Purdom, E.: Can we trust the bootstrap in high-dimension?, https://doi.org/10.48550/arXiv.1608.00696, 2 August 2016.

Keys, P. W. and Wang-Erlandsson, L.: On the social dynamics of moisture recycling, Earth System Dynamics, 9, 829–847, https://doi.org/10.5194/esd-9-829-2018, 2018.

Keys, P. W., van der Ent, R. J., Gordon, L. J., Hoff, H., Nikoli, R., and Savenije, H. H. G.: Analyzing precipitationsheds to understand the vulnerability of rainfall dependent regions, Biogeosciences, 9, 733–746, https://doi.org/10.5194/bg-9-733-2012, 2012.

Keys, P. W., Barnes, E. A., Van Der Ent, R. J., and Gordon, L. J.: Variability of moisture recycling using a precipitationshed framework, Hydrol. Earth Syst. Sci., 18, 3937–3950, https://doi.org/10.5194/hess-18-3937-2014, 2014.

Keys, P. W., Wang-Erlandsson, L., and Gordon, L. J.: Revealing Invisible Water: Moisture Recycling as an Ecosystem Service, PLoS ONE, 11, e0151993, https://doi.org/10.1371/journal.pone.0151993, 2016.

Klein, C. and Taylor, C. M.: Dry soils can intensify mesoscale convective systems, Proc. Natl. Acad. Sci. U.S.A., 117, 21132–21137, https://doi.org/10.1073/pnas.2007998117, 2020.

Li, M., Ma, Z., Wu, P., Liu, J., Lv, M., Yang, Q., and Han, Y.: Ecological Response to Climate Change Across China From Combined Soil Temperature and Moisture Changes, Earth and Space Science, 9, e2022EA002640, https://doi.org/10.1029/2022EA002640, 2022.

Li, X., Luo, M., Zhao, Y., Zhang, H., Ge, E., Huang, Z., Wu, S., Wang, P., Wang, X., and Tang, Y.: A daily high-resolution (1 km) human thermal index collection over the North China Plain from 2003 to 2020, Sci Data, 10, 634, https://doi.org/10.1038/s41597-023-02535-y, 2023.

Li, Y., Xu, R., Yang, Z., Zhou, S., Lu, M., Lin, H., Zi, S., and Su, R.: Upwind Moisture Controls on Interannual Variations of Precipitation and Vegetation in China's Drylands, Geophysical Research Letters, 51, e2024GL110997, https://doi.org/10.1029/2024GL110997, 2024.

Lu, H., Qin, Z., Lin, S., Chen, X., Chen, B., He, B., Wei, J., and Yuan, W.: Large influence of atmospheric vapor pressure deficit on ecosystem production efficiency, Nat Commun, 13, 1653, https://doi.org/10.1038/s41467-022-29009-w, 2022.

Lu, Y., Jiang, S., Ren, L., Zhang, L., Wang, M., Liu, R., and Wei, L.: Spatial and Temporal Variability in Precipitation Concentration over Mainland China, 1961–2017, Water, 11, 881, https://doi.org/10.3390/w11050881, 2019.

Ma, R., Feng, S., Jin, S., Sun, J., Fu, S., Sun, S., and Han, H.: Statistical Characteristics and Environmental Conditions of the Warm-Season Severe Convective Events over North China, Atmosphere, 12, 52, https://doi.org/10.3390/atmos12010052, 2021.

Maestre, F. T., Eldridge, D. J., Soliveres, S., Kéfi, S., Delgado-Baquerizo, M., Bowker, M. A., García-Palacios, P., Gaitán, J., Gallardo, A., Lázaro, R., and Berdugo, M.: Structure and Functioning of Dryland Ecosystems in a Changing World, Annu. Rev. Ecol. Evol. Syst., 47, 215–237, https://doi.org/10.1146/annurev-ecolsys-121415-032311, 2016.

Massman, W. J.: A non-equilibrium model for soil heating and moisture transport during extreme surface heating: the soil (heat–moisture–vapor) HMV-Model Version 1, Geoscientific Model Development, 8, 3659–3680, https://doi.org/10.5194/gmd-8-3659-2015, 2015.

McHugh, T. A., Morrissey, E. M., Reed, S. C., Hungate, B. A., and Schwartz, E.: Water from air: an overlooked source of moisture in arid and semiarid regions, Scientific Reports, 5, 13767, 2015.

Miralles, D. G., Gentine, P., Seneviratne, S. I., and Teuling, A. J.: Land–atmospheric feedbacks during droughts and heatwaves: state of the science and current challenges, Ann N Y Acad Sci, 1436, 19–35, https://doi.org/10.1111/nyas.13912, 2019.

Moch, J. M., Mickley, L. J., Keller, C. A., Bian, H., Lundgren, E. W., Zhai, S., and Jacob, D. J.: Aerosol-Radiation Interactions in China in Winter: Competing Effects of Reduced Shortwave Radiation and Cloud-Snowfall-Albedo Feedbacks Under Rapidly Changing Emissions, J Geophys Res Atmos, 127, e2021JD035442, https://doi.org/10.1029/2021JD035442, 2022.

Moore, R. A., Martinetti, D., Bigg, E. K., Christner, B. C., and Morris, C. E.: Climatic and landscape changes as drivers of environmental feedback that influence rainfall frequency in the United States, Glob Chang Biol, 27, 6381–6393, https://doi.org/10.1111/gcb.15876, 2021.

Ormaniec, W., Sussex, S., Lorch, L., Schölkopf, B., and Krause, A.: Standardizing Structural Causal Models, https://doi.org/10.48550/arXiv.2406.11601, 17 March 2025.

Palmquist, K. A., Schlaepfer, D. R., Bradford, J. B., and Lauenroth, W. K.: Spatial and ecological variation in dryland ecohydrological responses to climate change: implications for management, Ecosphere, 7, e01590, https://doi.org/10.1002/ecs2.1590, 2016.

Pranindita, A., Wang-Erlandsson, L., Fetzer, I., and Teuling, A. J.: Moisture recycling and the potential role of forests as moisture source during European heatwaves, Clim Dyn, 58, 609–624, https://doi.org/10.1007/s00382-021-05921-7, 2022.

Qian, W. and Lin, X.: Regional trends in recent temperature indices in China, Clim. Res., 27, 119–134, https://doi.org/10.3354/cr027119, 2004.

Quichimbo, E. A., Singer, M. B., Michaelides, K., Hobley, D. E. J., Rosolem, R., and Cuthbert, M. O.: DRYP 1.0: a parsimonious hydrological model of DRYland Partitioning of the water balance, Geosci. Model Dev., 14, 6893–6917, https://doi.org/10.5194/gmd-14-6893-2021, 2021.

Rahmati, M., Amelung, W., Brogi, C., Dari, J., Flammini, A., Bogena, H., Brocca, L., Chen, H., Groh, J., Koster, R. D., McColl, K. A., Montzka, C., Moradi, S., Rahi, A., Sharghi S., F., and Vereecken, H.: Soil Moisture Memory: State-Of-The-Art and the Way Forward, Reviews of Geophysics, 62, e2023RG000828, https://doi.org/10.1029/2023RG000828, 2024.

Ren, J., Yang, J., Wu, F., Sun, W., Xiao, X., and Xia, J. (Cecilia): Regional thermal environment changes: Integration of satellite data and land use/land cover, iScience, 26, 105820, https://doi.org/10.1016/j.isci.2022.105820, 2022.

Robinson, David. A., Jones, S. B., Lebron, I., Reinsch, S., Domínguez, M. T., Smith, A. R., Jones, D. L., Marshall, M. R., and Emmett, B. A.: Experimental evidence for drought induced alternative stable states of soil moisture, Sci Rep, 6, 20018, https://doi.org/10.1038/srep20018, 2016.

Schaefli, B., van der Ent, R. J., Woods, R., and Savenije, H. H. G.: An analytical model for soil-atmosphere feedback, Hydrology and Earth System Sciences, 16, 1863–1878, https://doi.org/10.5194/hess-16-1863-2012, 2012.

Schumacher, D. L., Keune, J., Dirmeyer, P., and Miralles, D. G.: Drought self-propagation in drylands due to land–atmosphere feedbacks, Nat. Geosci., 15, 262–268, https://doi.org/10.1038/s41561-022-00912-7, 2022.

Schwingshackl, C., Hirschi, M., and Seneviratne, S. I.: A theoretical approach to assess soil moisture–climate coupling across CMIP5 and GLACE-CMIP5 experiments, Earth System Dynamics, 9, 1217–1234, https://doi.org/10.5194/esd-9-1217-2018, 2018.

Sippel, S., Zscheischler, J., Heimann, M., Lange, H., Mahecha, M. D., van Oldenborgh, G. J., Otto, F. E. L., and Reichstein, M.: Have precipitation extremes and annual totals been increasing in the world's dry regions over the last 60 years?, Hydrology and Earth System Sciences, 21, 441–458, https://doi.org/10.5194/hess-21-441-2017, 2017.

Stacke, T. and Hagemann, S.: Lifetime of soil moisture perturbations in a coupled land–atmosphere simulation, Earth System Dynamics, 7, 1–19, https://doi.org/10.5194/esd-7-1-2016, 2016.

Tan, L., Cai, Y., An, Z., Yi, L., Zhang, H., and Qin, S.: Climate patterns in north central China during the last 1800 yr and their possible driving force, Climate of the Past, 7, 685–692, https://doi.org/10.5194/cp-7-685-2011, 2011.

Tuinenburg, O. A. and Staal, A.: Tracking the global flows of atmospheric moisture and associated uncertainties, Hydrol. Earth Syst. Sci., 24, 2419–2435, https://doi.org/10.5194/hess-24-2419-2020, 2020.

Tuinenburg, O. A., Theeuwen, J. J., and Staal, A.: High-resolution global atmospheric moisture connections from evaporation to precipitation, Earth System Science Data, 12, 3177–3188, 2020.

Van Der Ent, R. J., Wang-Erlandsson, L., Keys, P. W., and Savenije, H. H. G.: Contrasting roles of interception and transpiration in the hydrological cycle – Part 2: Moisture recycling, Earth Syst. Dynam., 5, 471–489, https://doi.org/10.5194/esd-5-471-2014, 2014.

Wang, L., D'Odorico, P., Evans, J. P., Eldridge, D. J., McCabe, M. F., Caylor, K. K., and King, E. G.: Dryland ecohydrology and climate change: critical issues and technical advances, Hydrol. Earth Syst. Sci., 16, 2585–2603, https://doi.org/10.5194/hess-16-2585-2012, 2012.

Wang, Q., Ju, Q., Wang, Y., Shao, Q., Zhang, R., Liu, Y., and Hao, Z.: Vegetation Changing Patterns and Its Sensitivity to Climate Variability across Seven Major Watersheds in China, Int J Environ Res Public Health, 19, 13916, https://doi.org/10.3390/ijerph192113916, 2022.

Wu, H., Xu, X., and Wang, Y.: Effects of Orography on the High-Temperature Event on 22 June 2023 in North China, Atmosphere, 15, 324, https://doi.org/10.3390/atmos15030324, 2024.

Wunderling, N., Wolf, F., Tuinenburg, O. A., and Staal, A.: Network motifs shape distinct functioning of Earth's moisture recycling hubs, Nature Communications, 13, 6574, https://doi.org/10.1038/s41467-022-34229-1, 2022.

Xu, Z., Chen, H., Guo, J., and Zhang, W.: Contrasting Effect of Soil Moisture on the Daytime Boundary Layer Under Different Thermodynamic Conditions in Summer Over China, Geophysical Research Letters, 48, e2020GL090989, https://doi.org/10.1029/2020GL090989, 2021.

Yang, L., Sun, G., Zhi, L., and Zhao, J.: Negative soil moisture-precipitation feedback in dry and wet regions, Sci Rep, 8, 4026, https://doi.org/10.1038/s41598-018-22394-7, 2018.

Yin, J. and Porporato, A.: Coupling hotspots: distinguishing between positive and negative land-atmosphere interaction, https://doi.org/10.48550/arXiv.2412.03049, 4 December 2024.

Zhang, K., Chen, H., Ma, N., Shang, S., Wang, Y., Xu, Q., and Zhu, G.: A global dataset of terrestrial evapotranspiration and soil moisture dynamics from 1982 to 2020, Sci Data, 11, 445, https://doi.org/10.1038/s41597-024-03271-7, 2024.

Zhang, R., Chu, Q., Zuo, Z., and Qi, Y.: Summertime Moisture Sources and Transportation Pathways for China and Associated Atmospheric Circulation Patterns, Front. Earth Sci., 9, https://doi.org/10.3389/feart.2021.756943, 2021.

Zhang, S., Meurey, C., and Calvet, J.-C.: Identification of soil-cooling rains in southern France from soil temperature and soil moisture observations, Atmospheric Chemistry and Physics, 19, 5005–5020, https://doi.org/10.5194/acp-19-5005-2019, 2019.

Zhao, C., Yao, S., Liu, J., and Wang, J.: The Spatial Distribution of Precipitation in Northwest China, Journal of Electrical and Computer Engineering, 2014, 514291, https://doi.org/10.1155/2014/514291, 2014.